Low Frequency Receiver - LFR

In-flight performance and observations of whistler mode waves

Thomas Chust, the LFR team and the RPW instrument consortium

The instrument

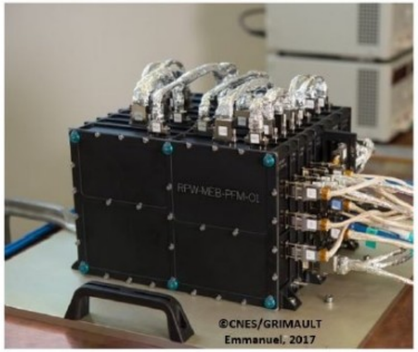

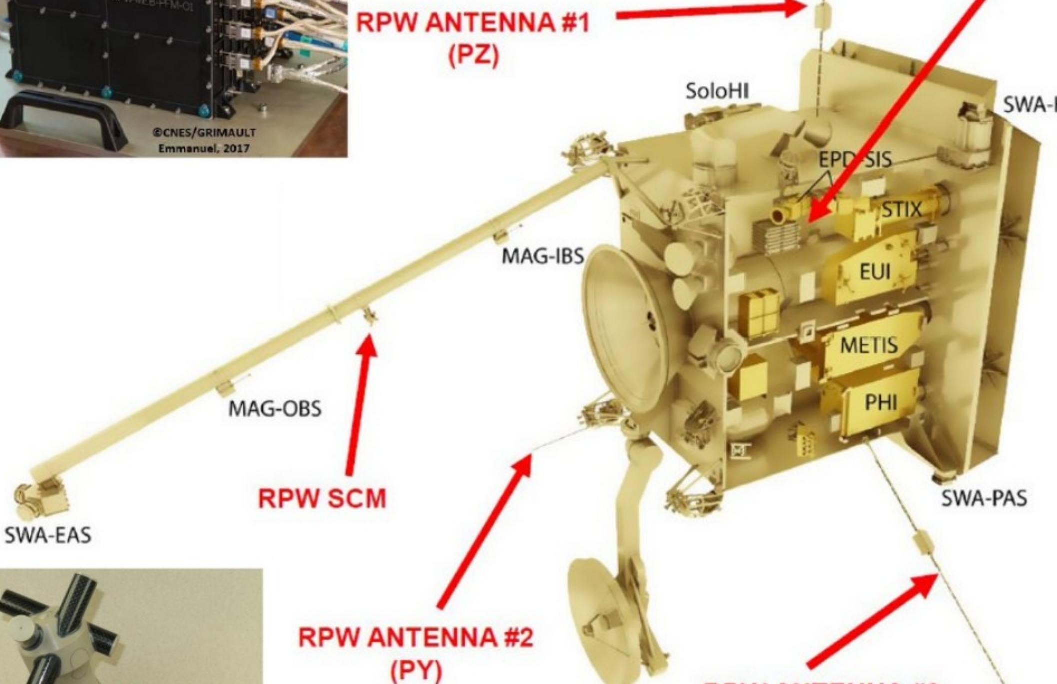

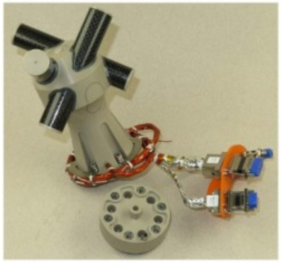

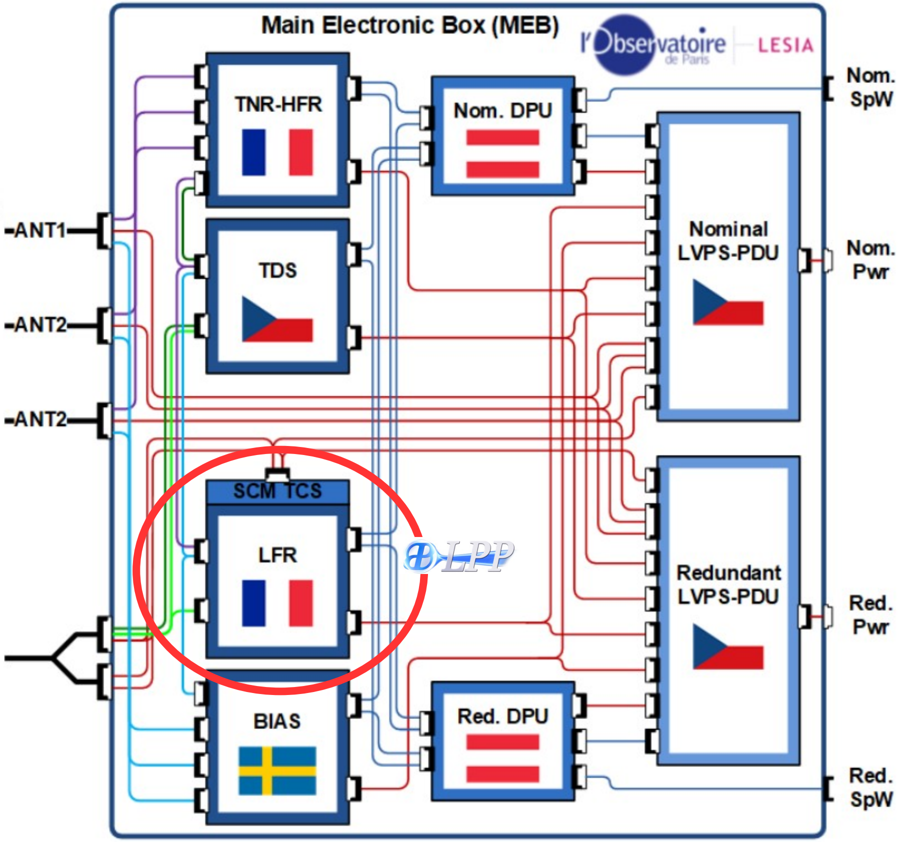

RPW Instrument Overview

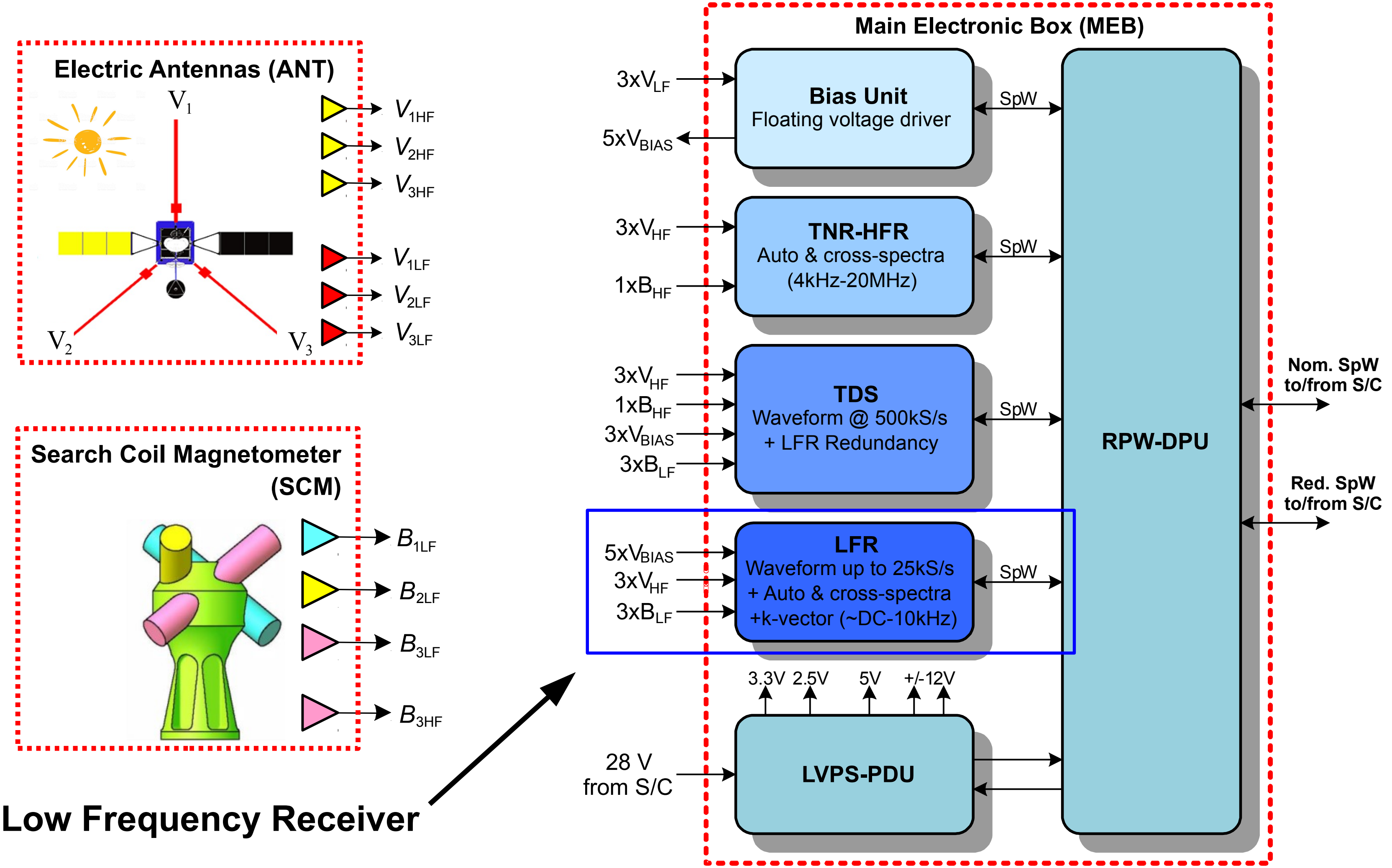

Low Frequency Receiver

Solar Orbiter's RPW Low Frequency Receiver (LFR)

LFR nominal inputs : **3 B + 2 E + 1 V (≤ 10 kHz)**,

The LFR signal processing, based on a FPGA, provides routinely,
- waveforms (SWF & CWF)
- spectral matrices (ASM & BP2)
- basic wave parameters (BP1)

at different time and frequency resolutions:

LFR Normal Mode data flow

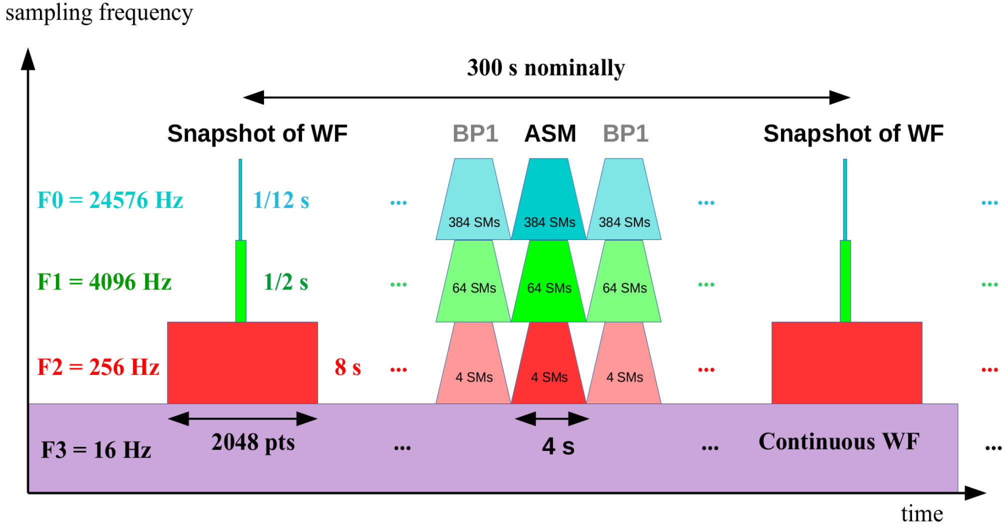

LFR data are calibrated at LESIA by the **ROC production pipeline**, using the calibration softwares of the teams (SCM, BIAS & LFR):
- SCMCAL (LPCE2, Orléans, France)
- BICAS (IRF, Uppsala, Sweden)
- LFR-CALBUT (LPP, Palaiseau, France)

Despite the fact that calibrations of the E and B data still require some improvement (phase shift issue, effective antenna lengths), the first results obtained so far show a **good overall consistency of the RPW LFR data** (A&A 2021 special issue papers, about 12 papers)

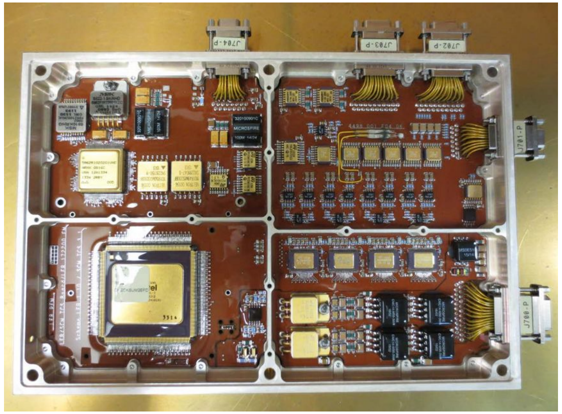

LFR FM board

Astronomy & Astrophysics manuscript no. aa40932-21
November 7, 2021

Solar Orbiter First Results (Cruise Phase)

Special issue

Observations of whistler mode waves by Solar Orbiter's RPW Low Frequency Receiver (LFR): In-flight performance and first results

T. Chust[1], M. Kretzschmar[2], D. B. Graham[3], O. Le Contel[1], A. Retinò[1], A. Alexandrova[1], M. Berthomier[1], L. Z. Hadid[1], F. Sahraoui[1], A. Jeandet[1], P. Leroy[1], J.-C. Pellion[1], V. Bouzid[1], B. Katra[1], R. Piberne[1], Yu. V. Khotyaintsev[3], A. Vaivads[3,4], V. Krasnoselskikh[2], J. Souček[5], O. Santolík[5,6], E. Lorfèvre[7], D. Plettemeier[8], M. Steller[9], Š. Štverák[10], P. Trávníček[13,10], A. Vecchio[11,12], M. Maksimovic[11], S. D. Bale[13,14,15], T. S. Horbury[16], H. O'Brien[16], V. Evans[16], and V. Angelini[16]

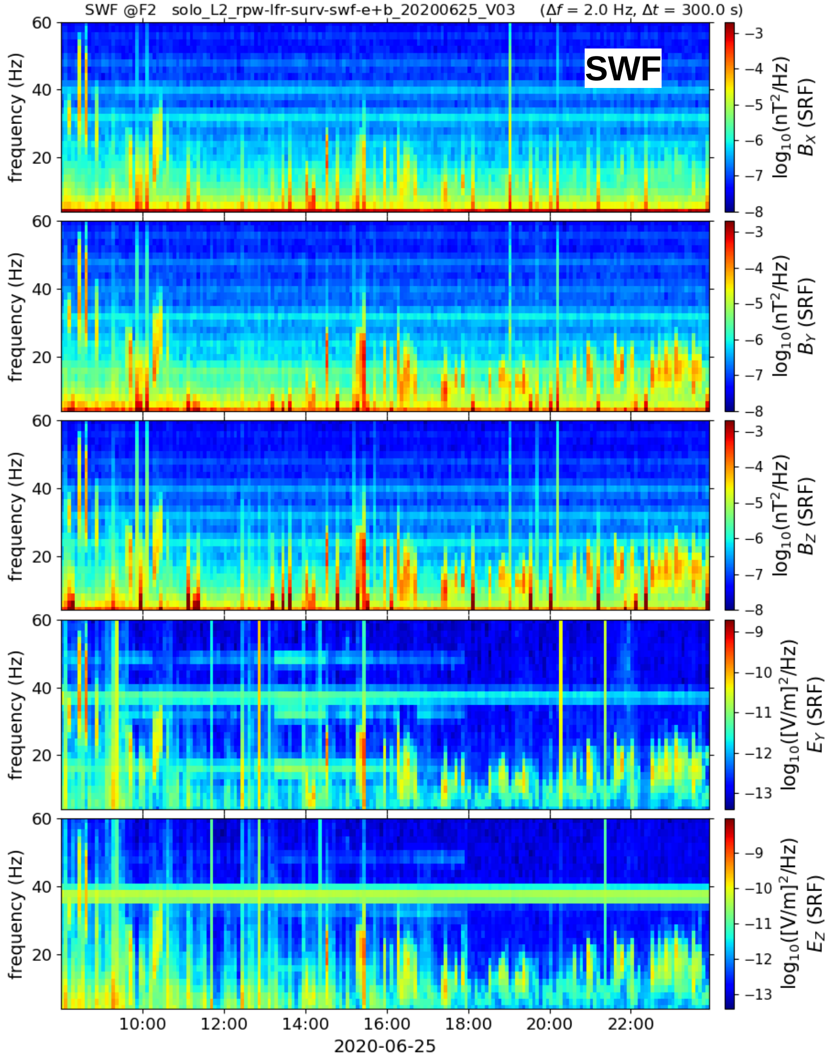

PSD computed from the snapshots of WF (every 300 s, Δ*f* = 2Hz) compared with the PSD computed onboard (every 20 s, Δ*f* = 8 Hz, BP2 data set)

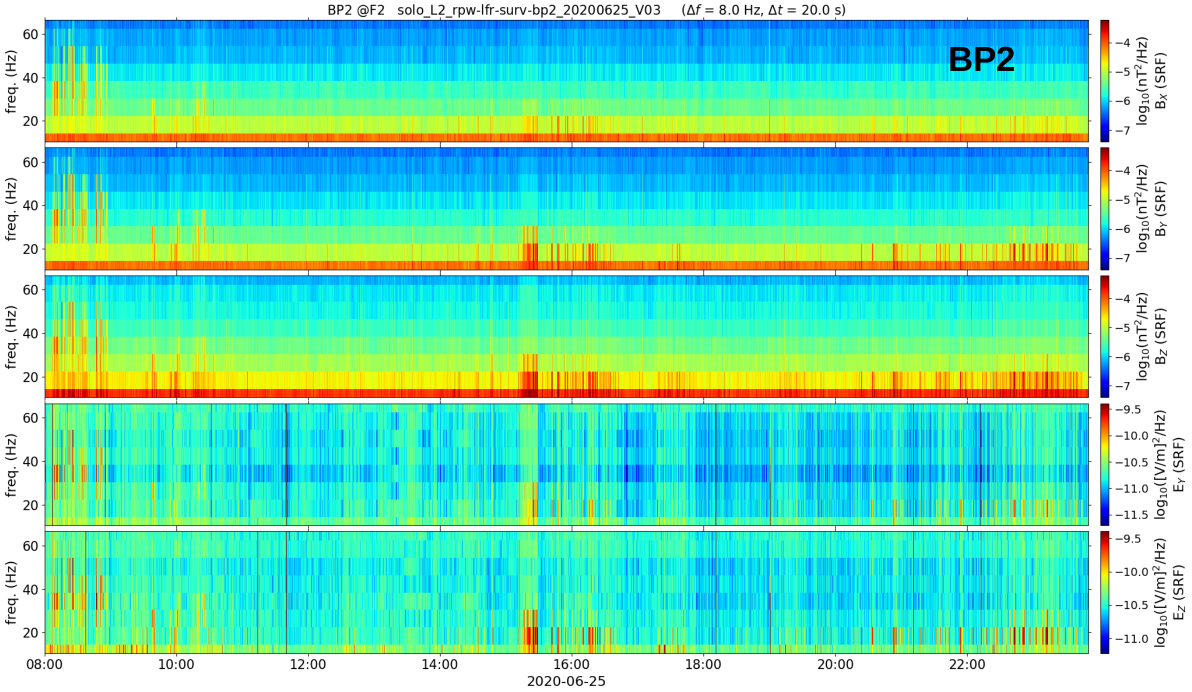

Chust et al. A&A 2021

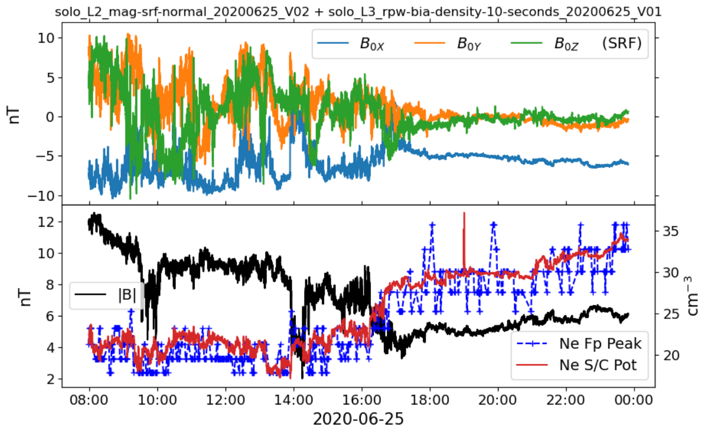

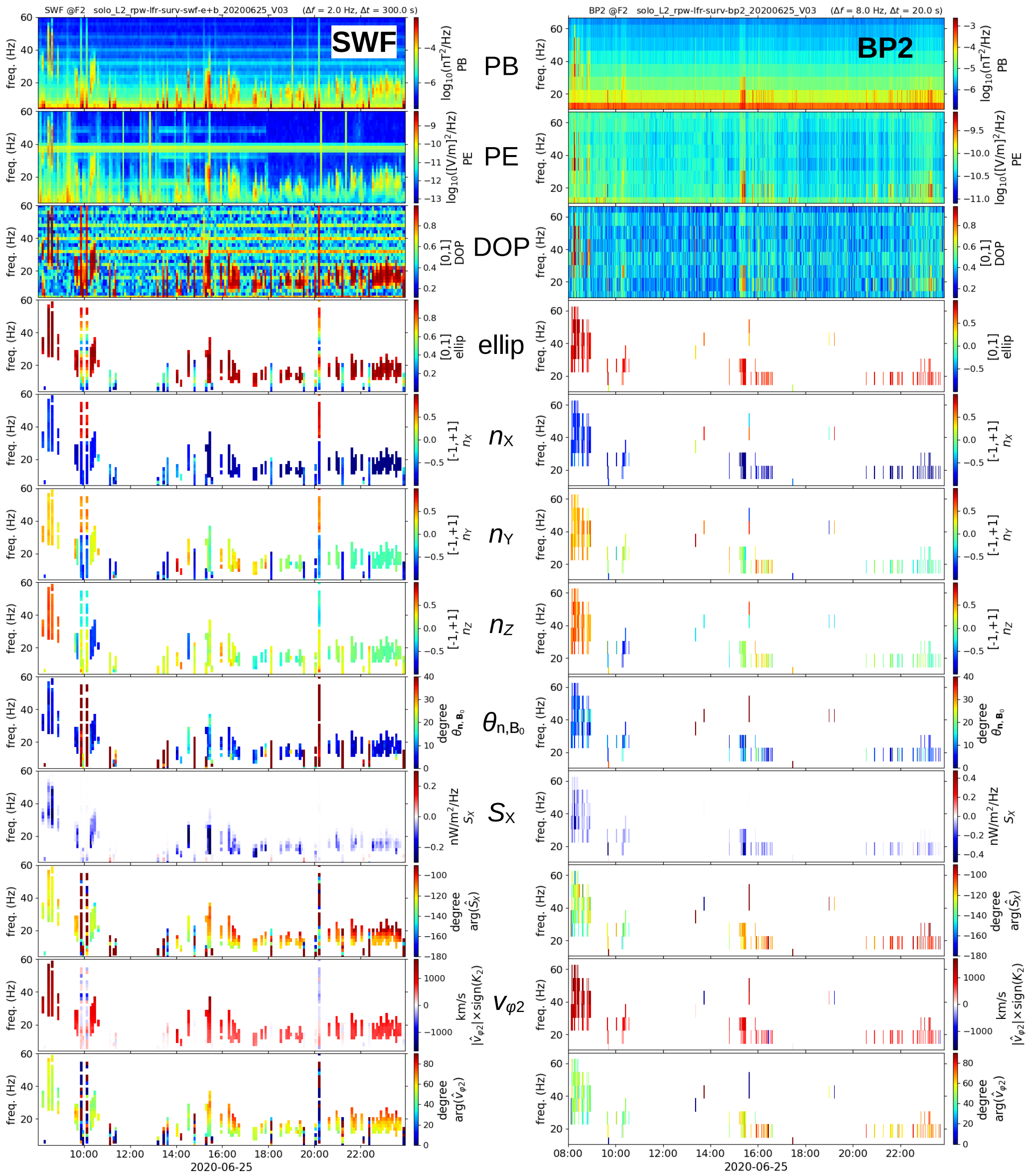

$$\left.\begin{array}{l} \mathbf{n}\times\tilde{\mathbf{E}} = \dfrac{\omega}{K}\tilde{\mathbf{B}} \\ \tilde{\mathbf{E}}\cdot\mathbf{B}_0 = 0 \end{array}\right\} \Rightarrow \tilde{\mathbf{E}} = -\frac{\omega}{K}\,\frac{\mathbf{B}_0\times\tilde{\mathbf{B}}}{\mathbf{n}\cdot\mathbf{B}_0}$$

$$\frac{\omega}{K} \approx \frac{(\mathbf{n}\cdot\mathbf{B}_0)\left\langle \hat{E}_Y\hat{B}_Y^*\right\rangle_t/\rho_{E_YB_Y}}{B_{0X}\left\langle \hat{B}_Z\hat{B}_Y^*\right\rangle_t/\rho_{B_ZB_Y} - B_{0Z}\left\langle \hat{B}_X\hat{B}_Y^*\right\rangle_t/\rho_{B_XB_Y}} = \hat{v}_{\varphi 2}(\omega)$$

with **n**, the wave normal vector (Means, JGR, 1972),

and : $\mathbf{k} = \mathbf{n}\times K$

$$\rho_{ij} = \frac{\left|\left\langle \hat{P}_i\hat{P}_j^*\right\rangle_t\right|}{\sqrt{\left\langle \hat{P}_i\hat{P}_i^*\right\rangle_t\left\langle \hat{P}_j\hat{P}_j^*\right\rangle_t}}$$

Chust et al. A&A 2021

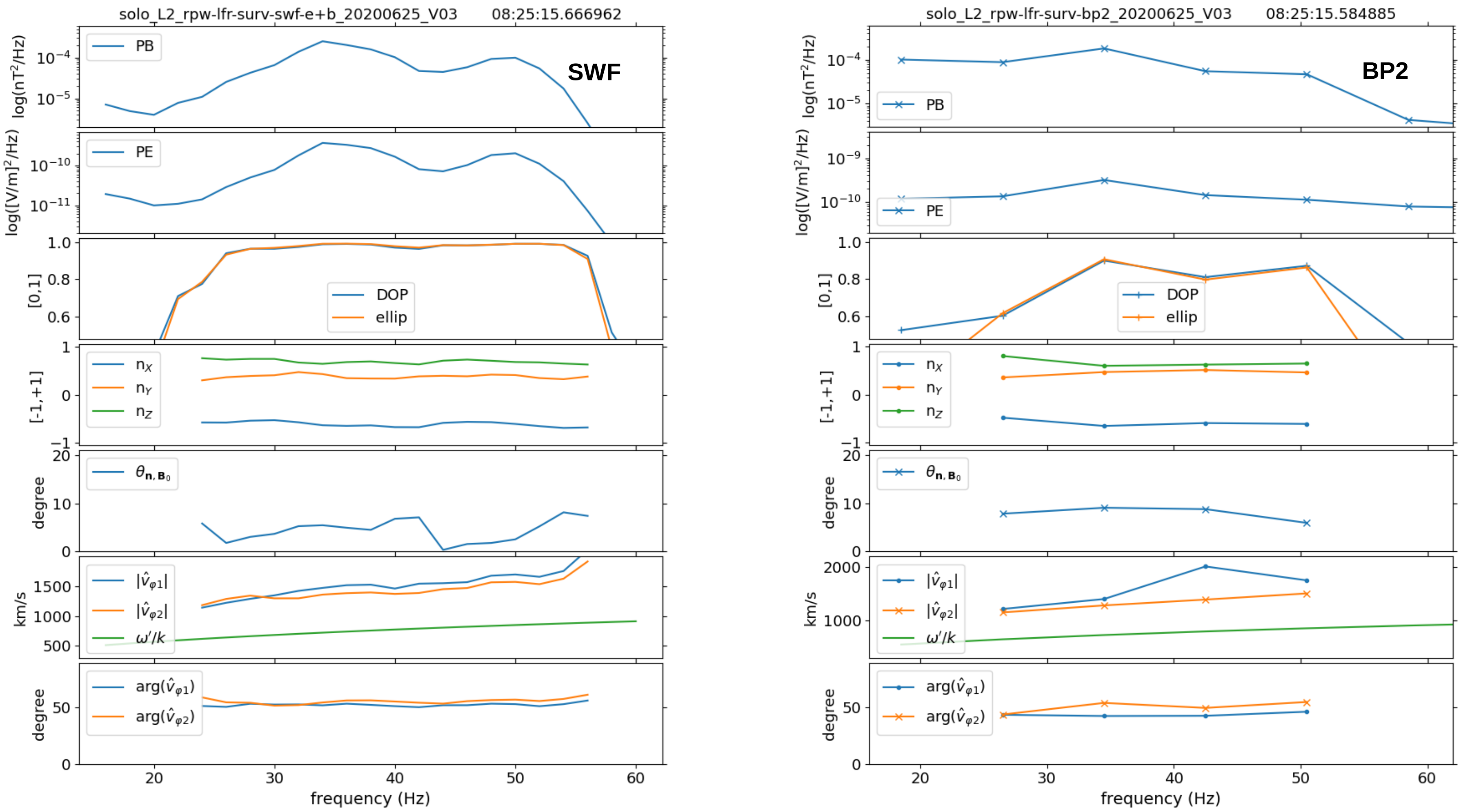

$$\frac{\omega}{K} \approx \frac{n_Y \left\langle \hat{E}_Z \hat{B}_X^* \right\rangle_t / \rho_{E_Z B_X} - n_Z \left\langle \hat{E}_Y \hat{B}_X^* \right\rangle_t / \rho_{E_Y B_X}}{\left\langle \hat{B}_X \hat{B}_X^* \right\rangle_t} = \hat{v}_{\varphi 1}(\omega)$$

Chust et al. A&A 2021

Identification of whistler mode waves in the solar wind

Phase velocity measured (orange) from waveforms (SWF data set) compared with the theoretical (red) Doppler shifted (+**k**) whistler mode

Phase velocity measured (orange) from onboard spectral data products (BP2 data set) compared with the theoretical (red) Doppler shifted (+**k**) whistler mode

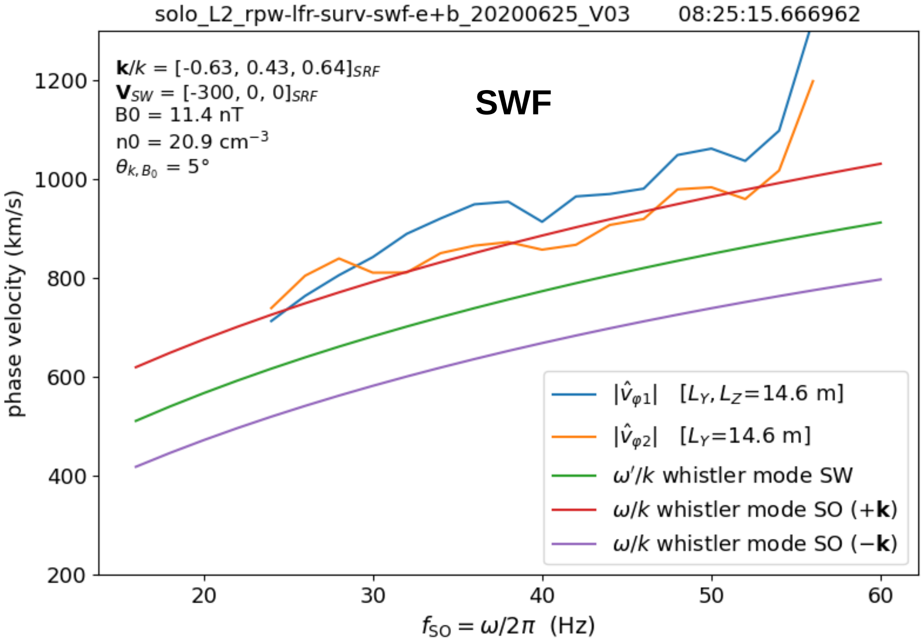

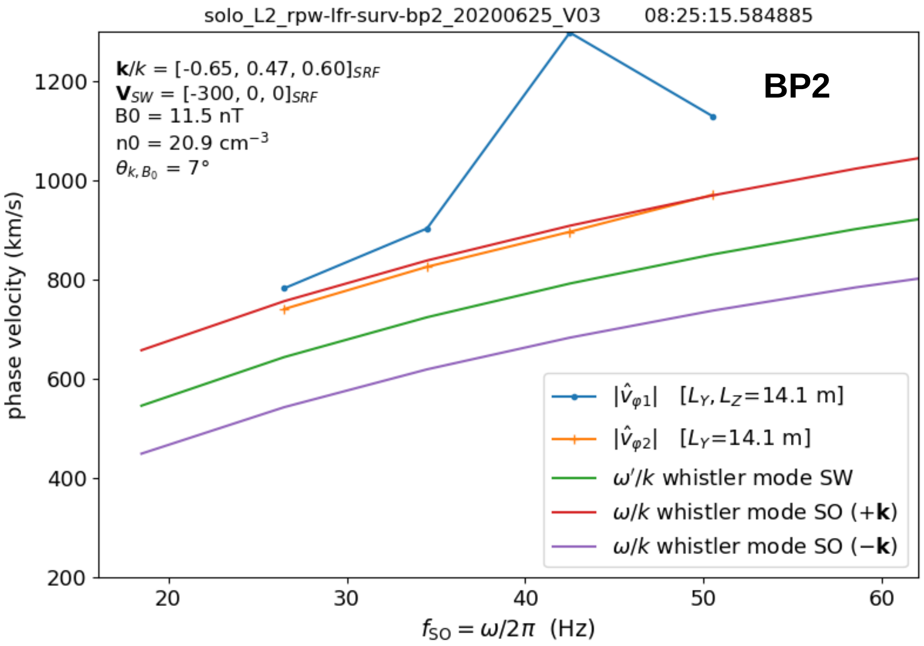

$$\omega = \omega' + \mathbf{k} \cdot \mathbf{V}_{SW}$$

Chust et al. A&A 2021

Wave parameters computed onboard (every 4 s, Δf = 8Hz, BP1 data set) compared with those computed from the BP2 data set (every 20 s, Δf = 8 Hz)

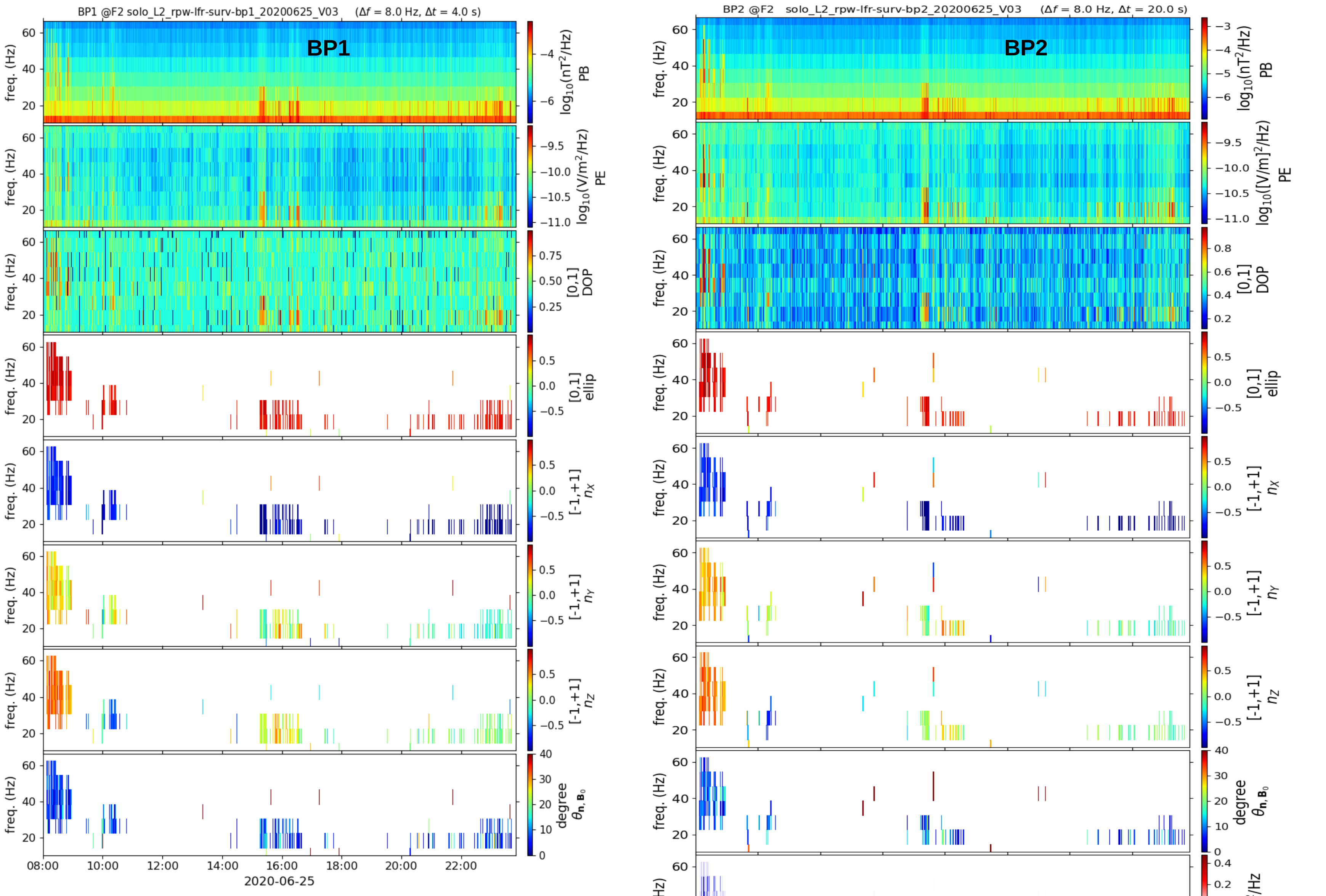

Chust et al.
A&A 2021

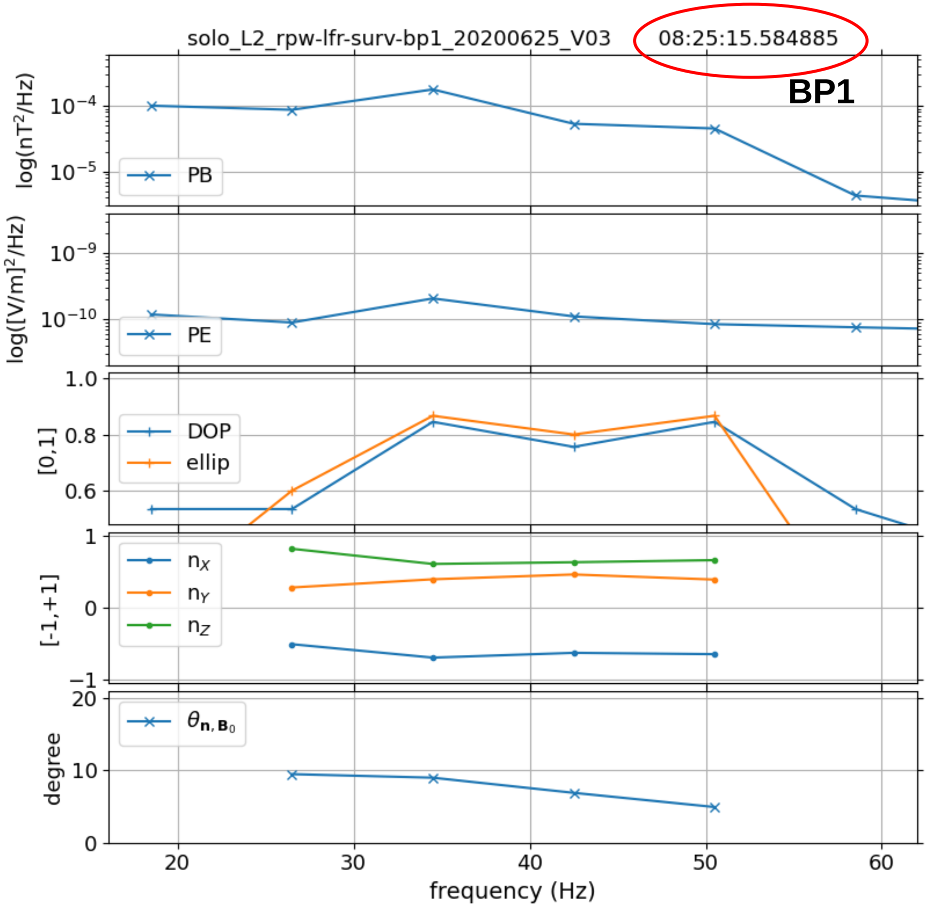

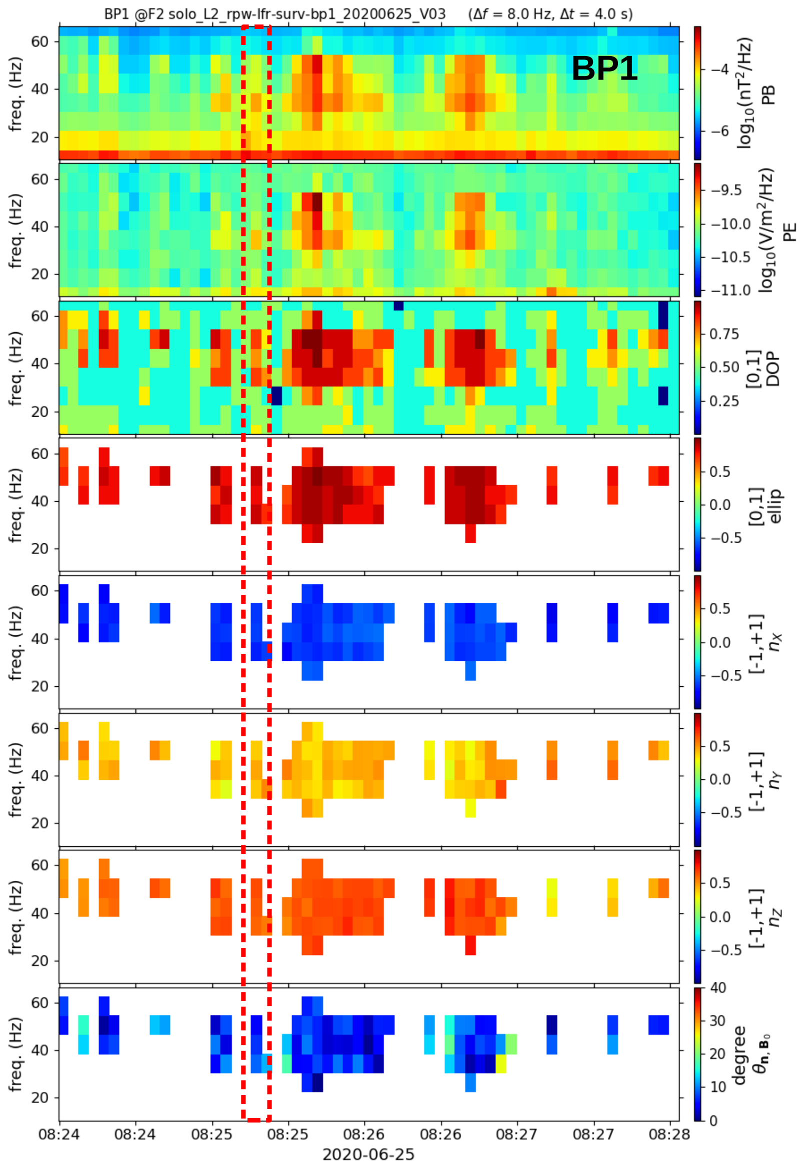

Chust et al. A&A 2021

Illustration again of the intermittency of the whistler mode waves and the correct calculation of BP1 data, but this time including the **Poynting flux S_X**, showing that the <u>update of the kcoefficients</u> worked very well

04:26:44 UTC (August 27, 2020)

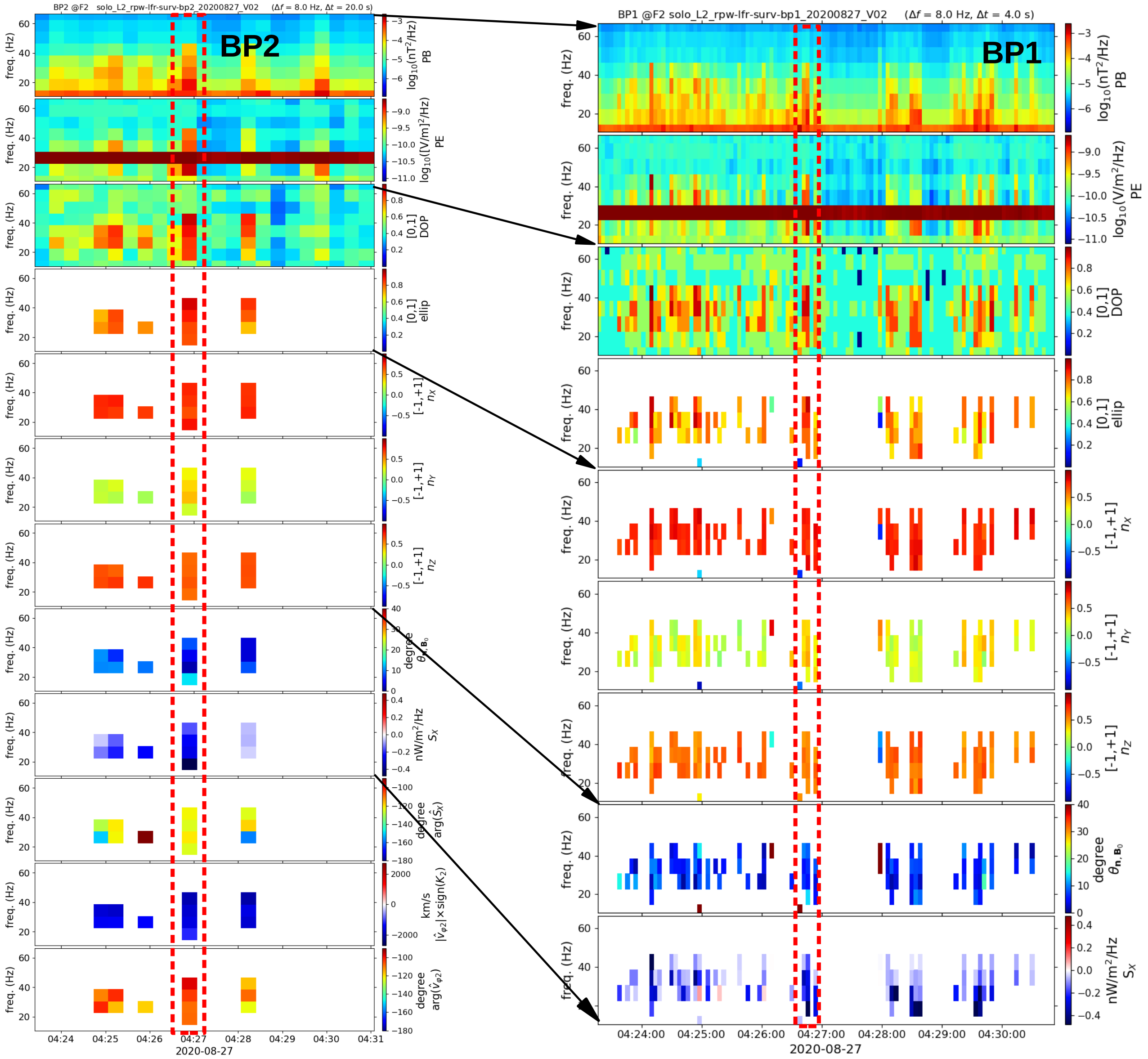

Chust et al. A&A 2021

Further verification of the consistency of the LFR data

SWF

F2 = 256 Hz

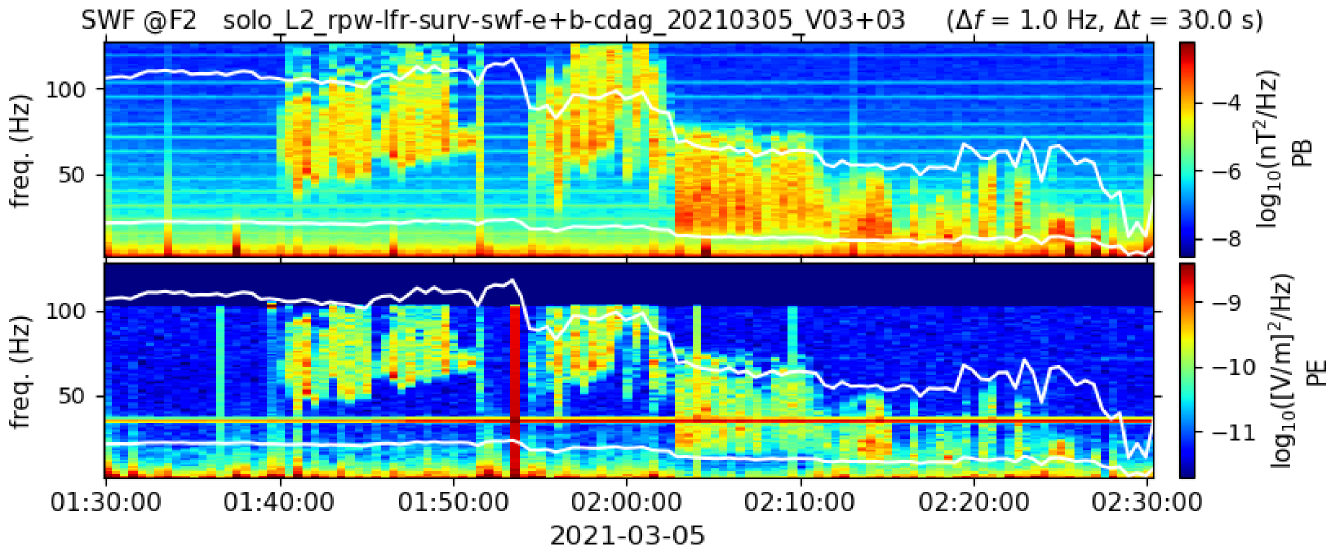

versus

F1 = 4096 HZ

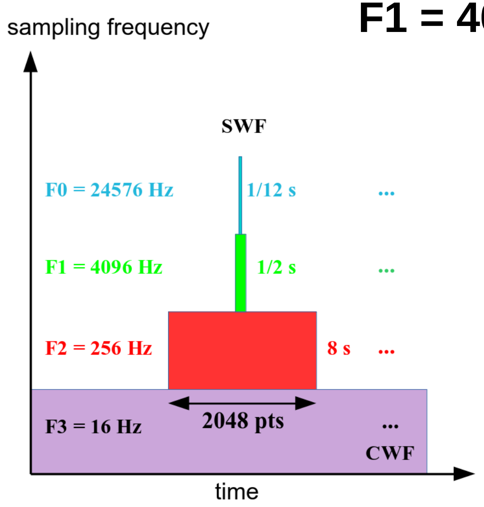

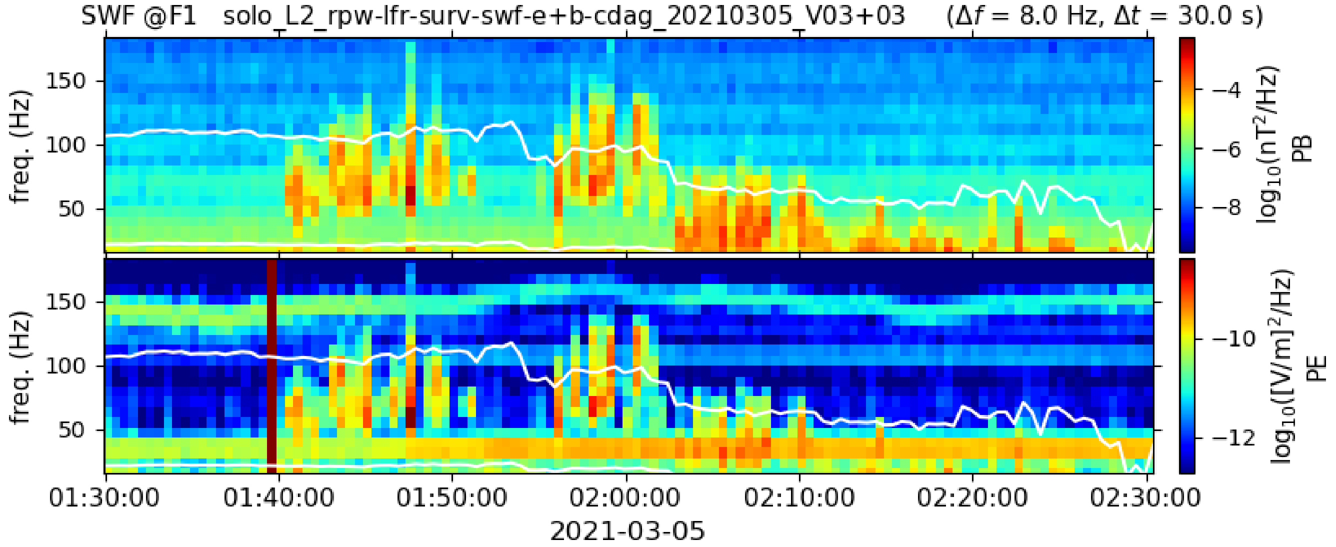

SWF

F2 versus F1

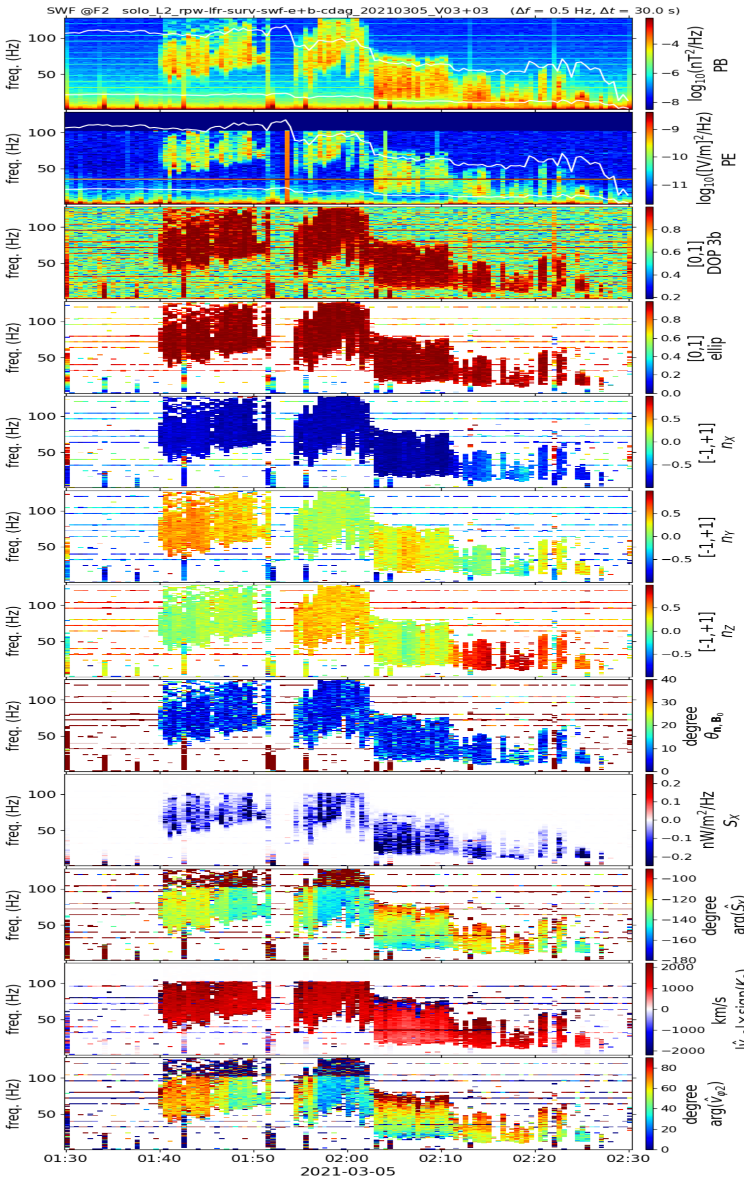

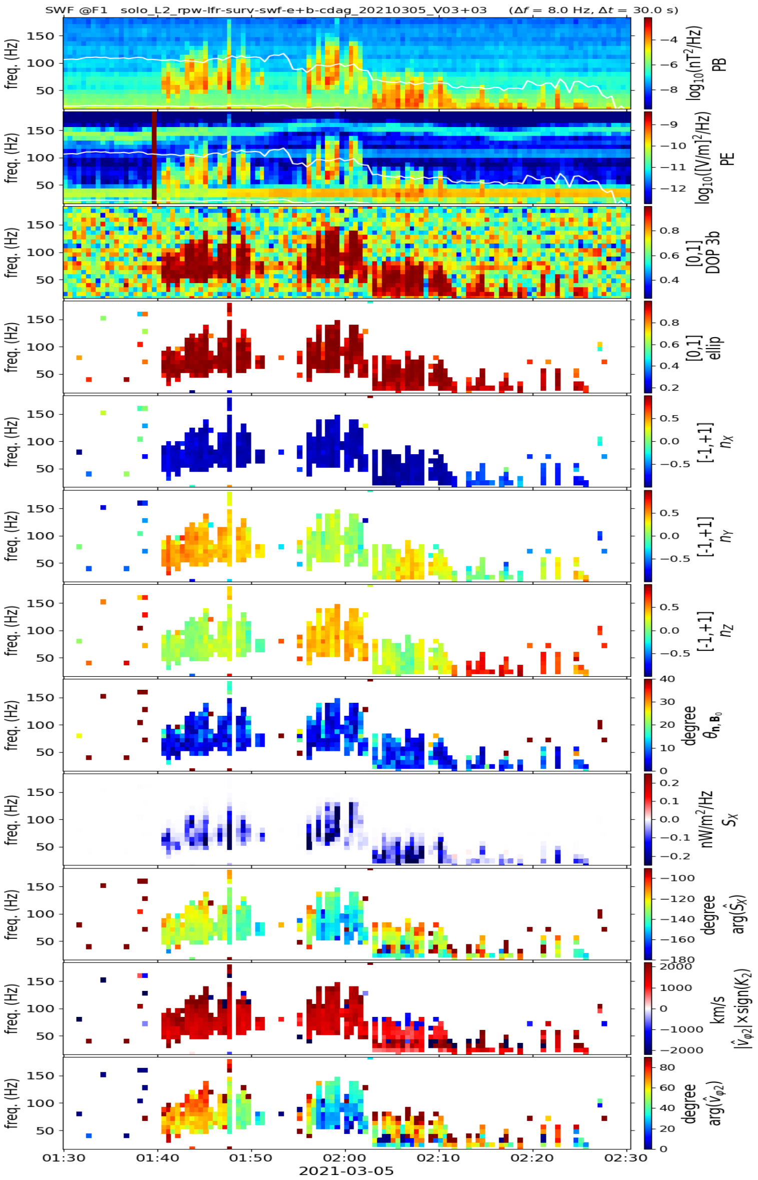

SWF

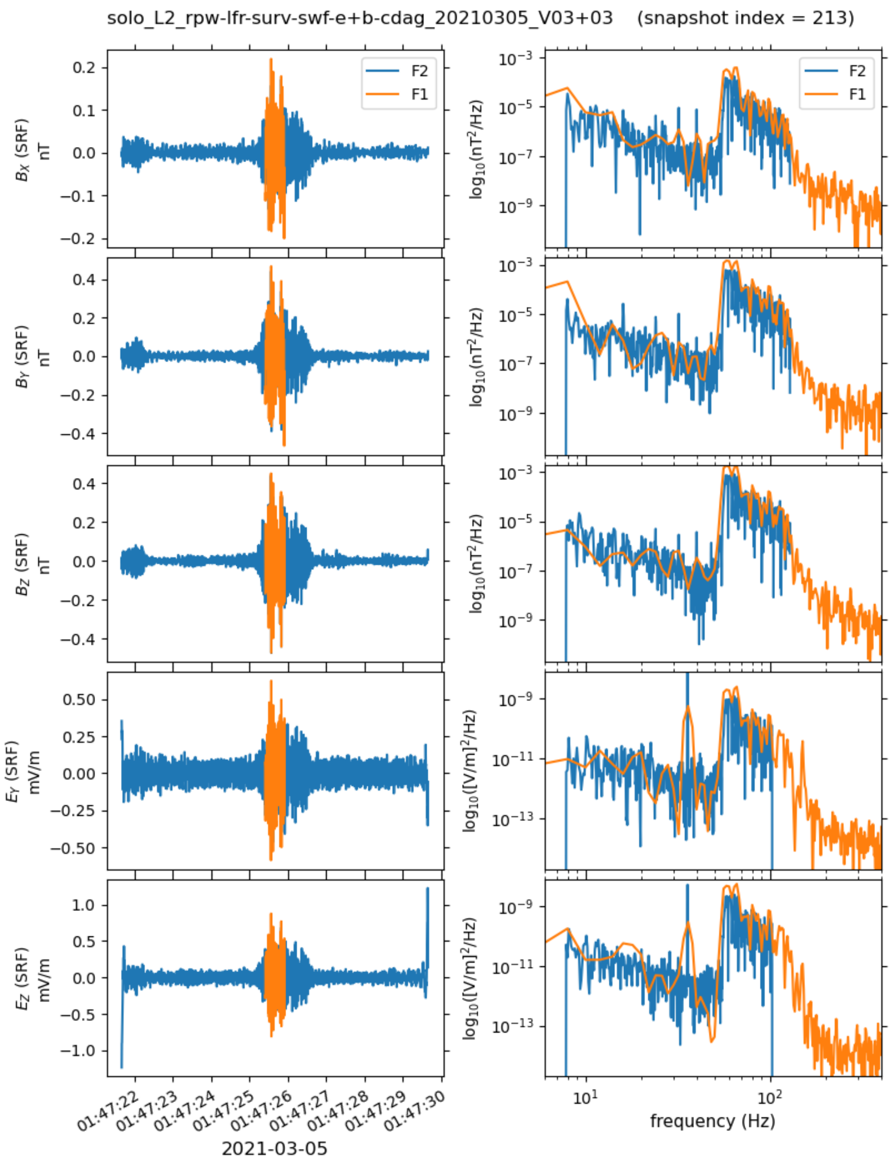

F2 versus F1

zoom :

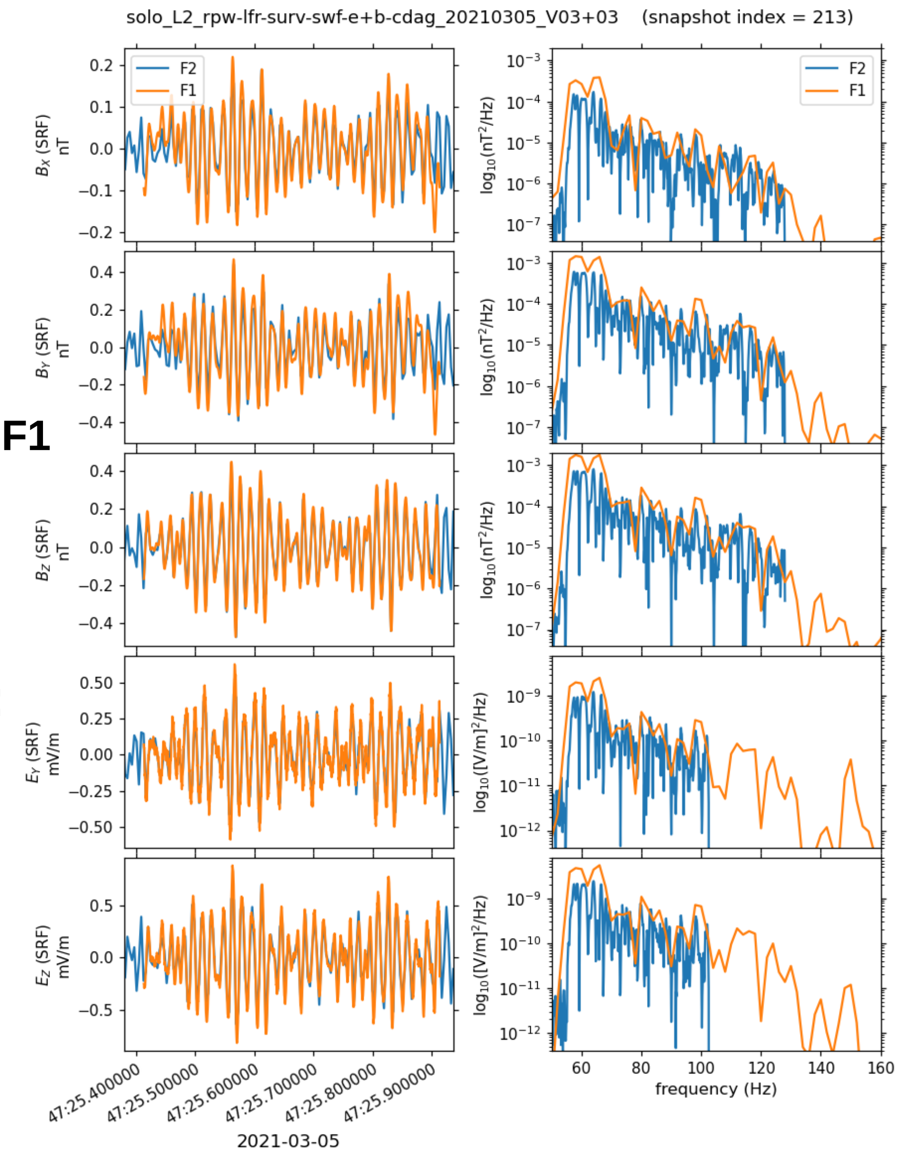

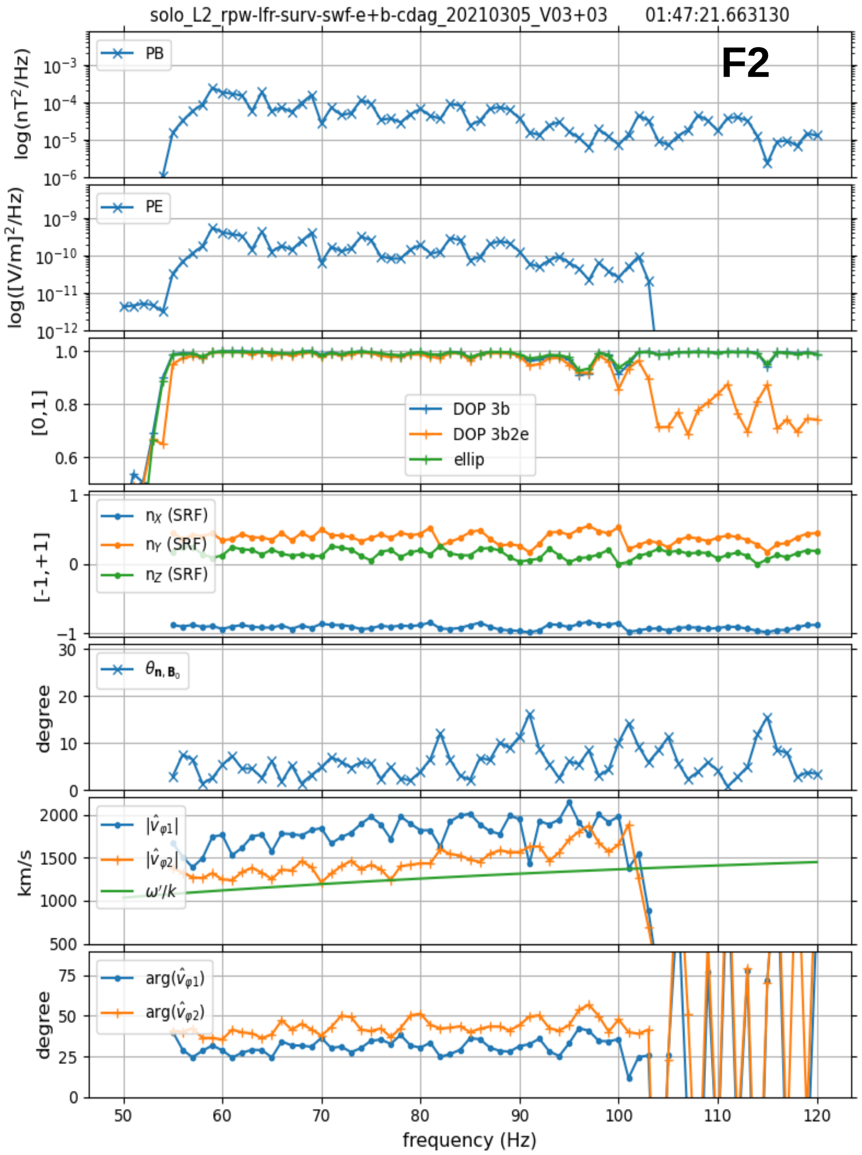

SWF

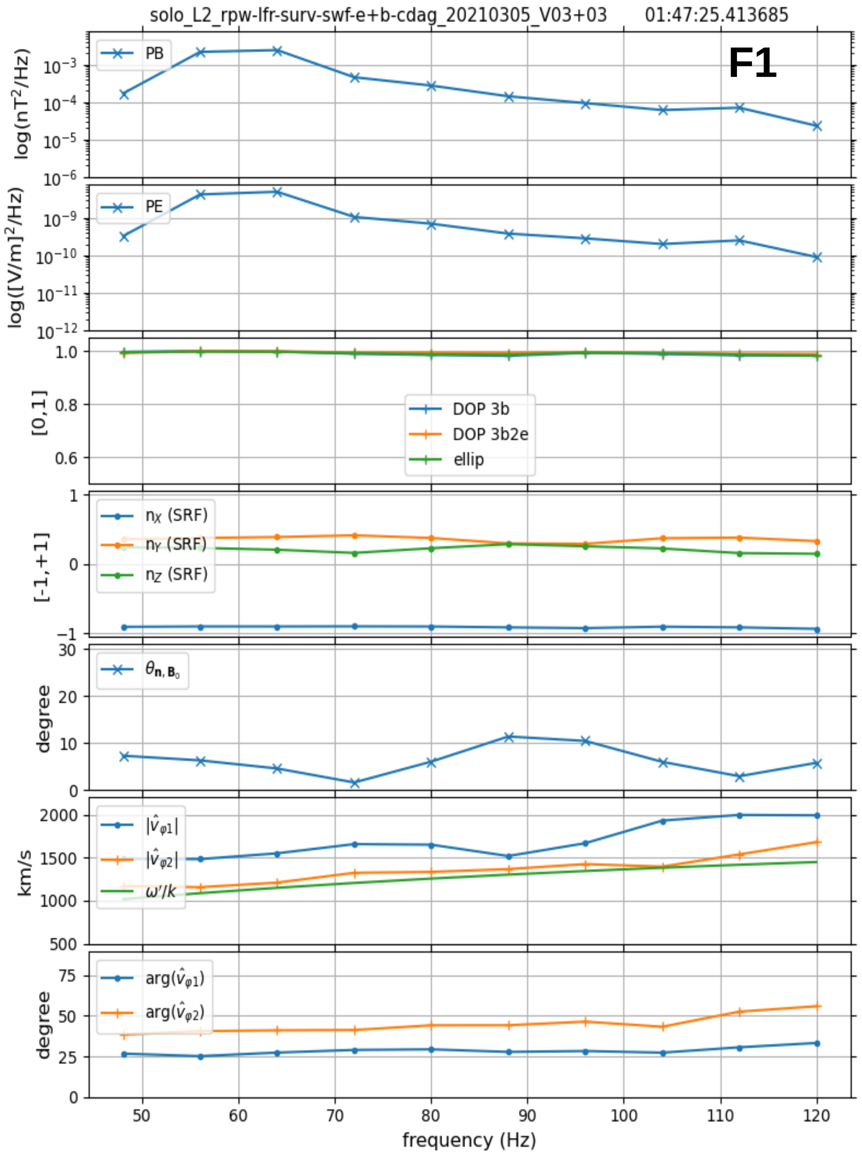

F2 versus F1

Caveat : due to the intermittency features, the PSDs show differences even though the wave propagation characteristics are similar.

F2

ASM

versus

SWF

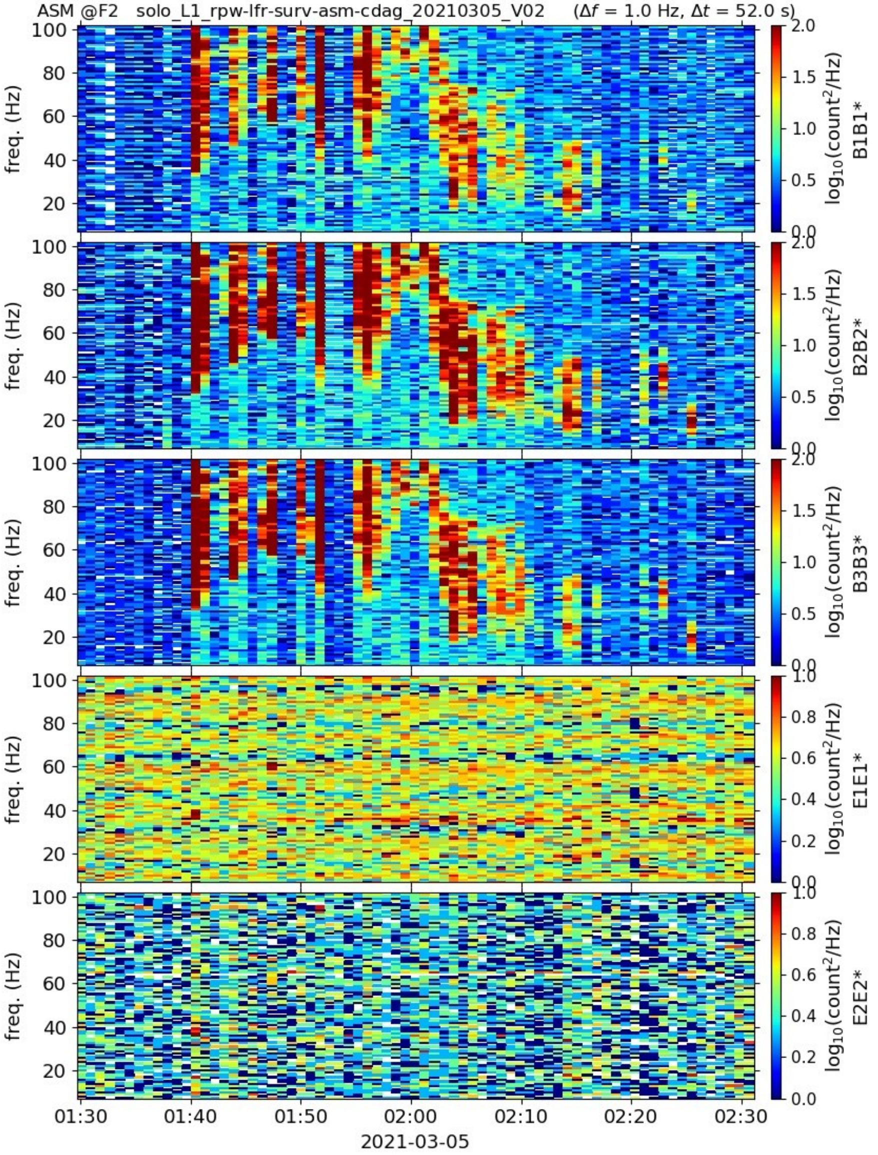

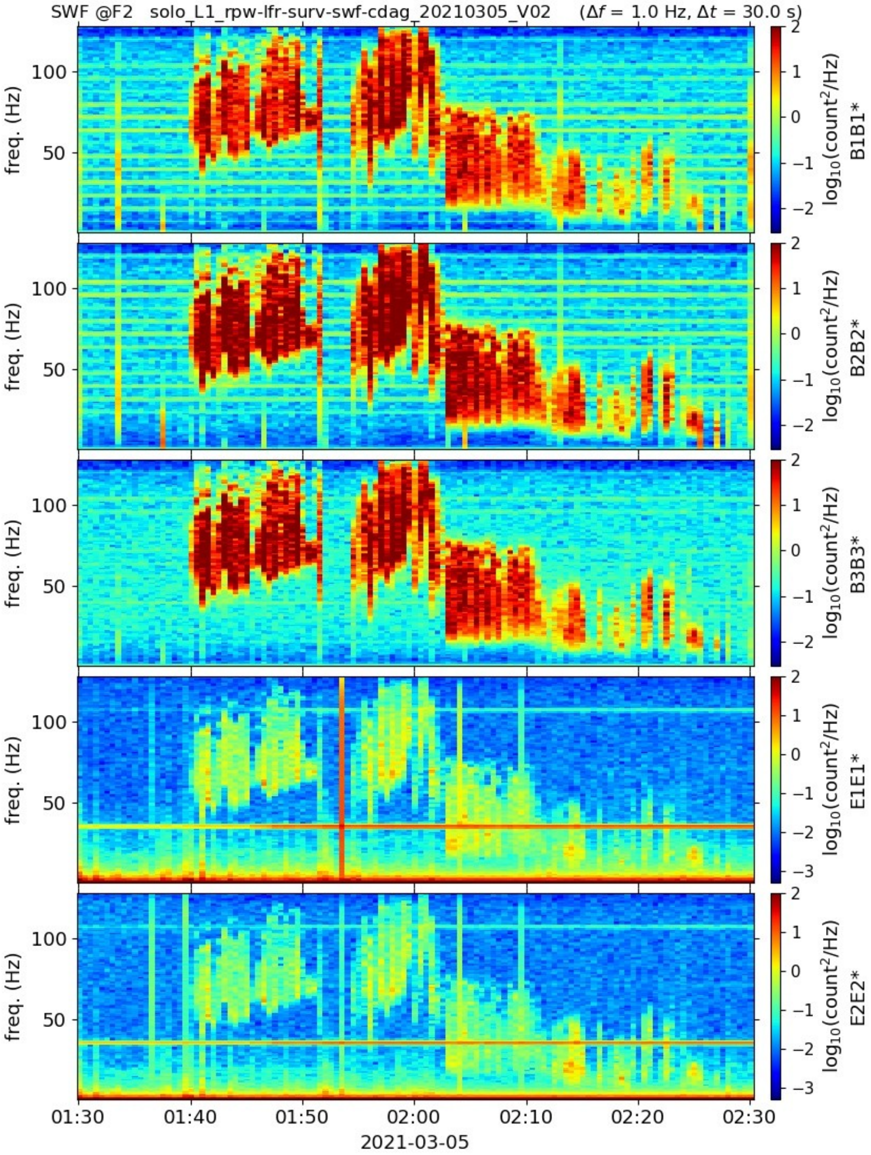

F2

ASM versus SWF

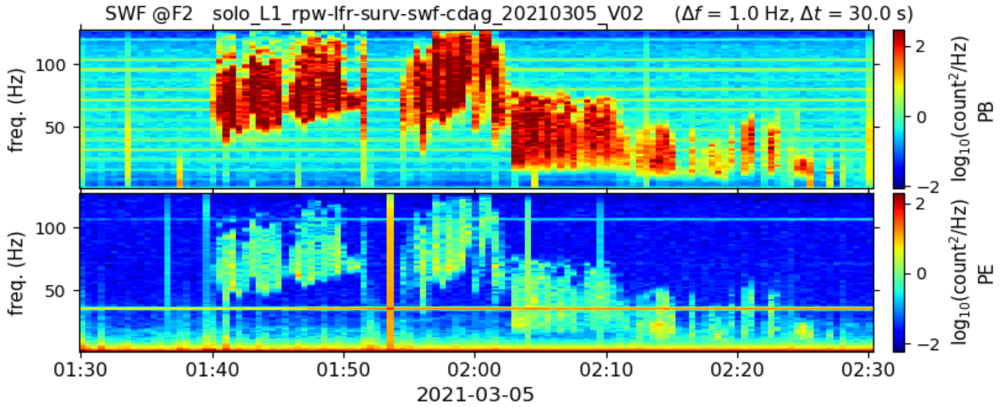

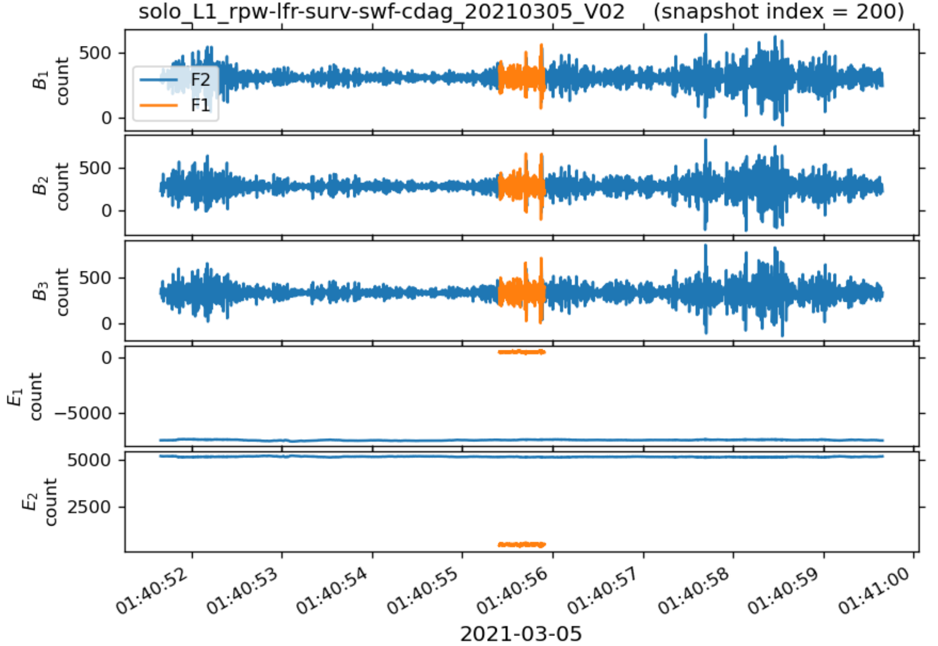

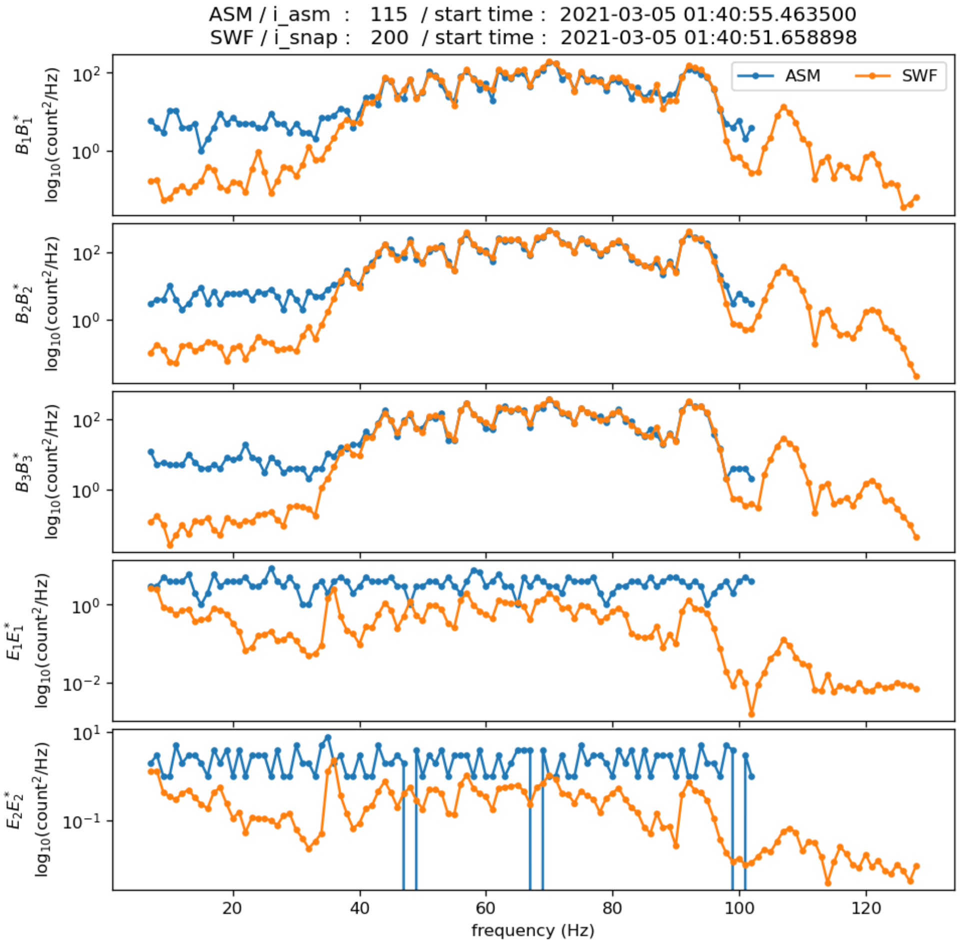

ASM versus SWF

F2

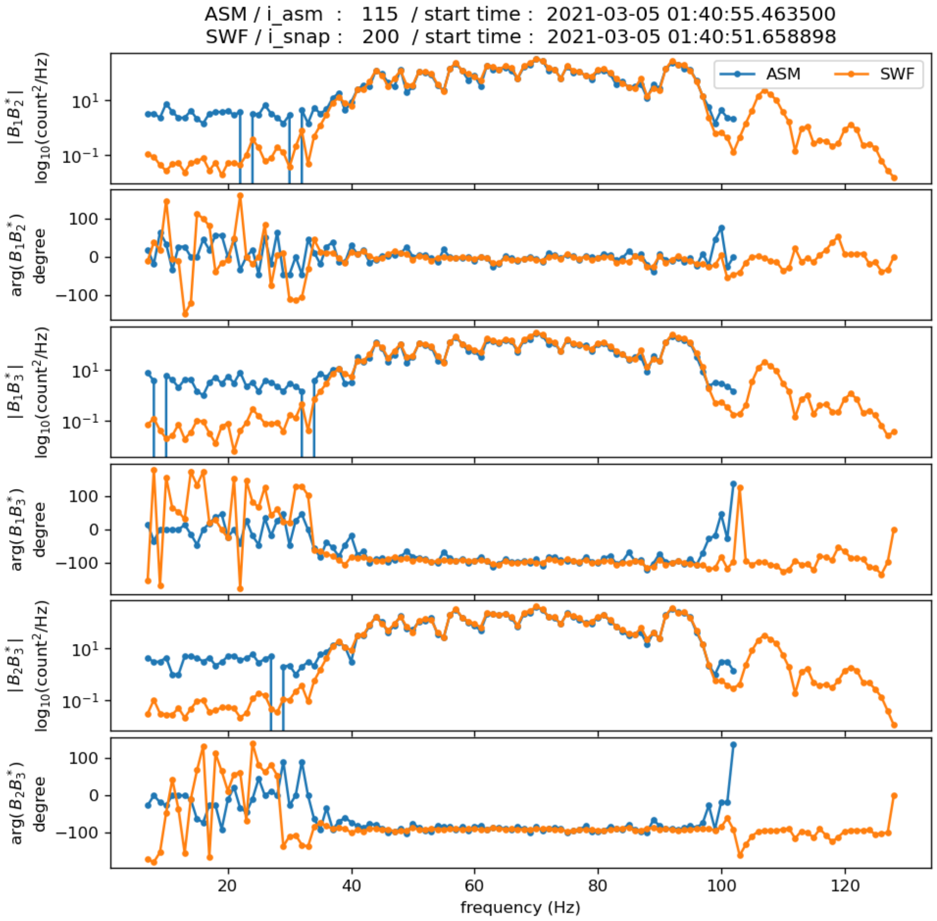

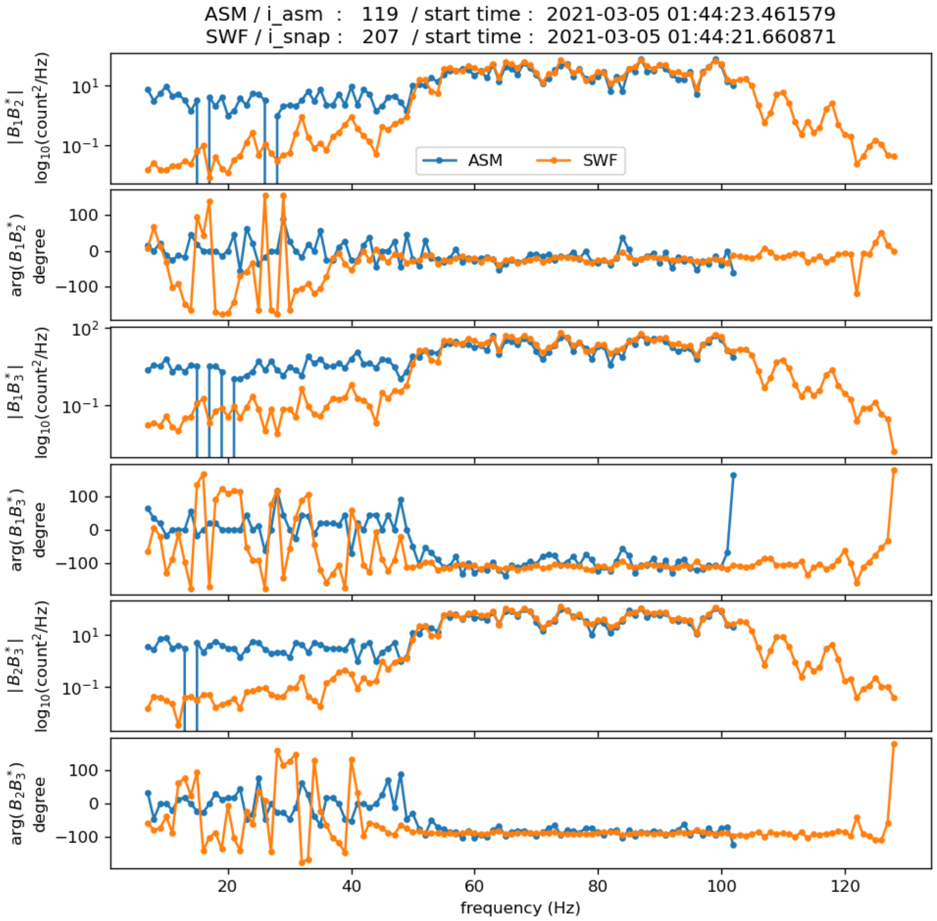

Conclusion

- Where possible, comparisons between all LFR data products show a **very good consistency**
- So far, **phase shift issue (between E and B) can be neglected** when determining the sign of S_X or the direction of the wave propagation (Kretzschmar et al. 2021; Chust et al. 2021).
- **Fluctuations in the determination of the effective antenna lengths** are still not well understood (Steinvall et al. 2021; Kretzschmar et al. 2021; Chust et al. 2021).

Additional slides

LFR block diagram

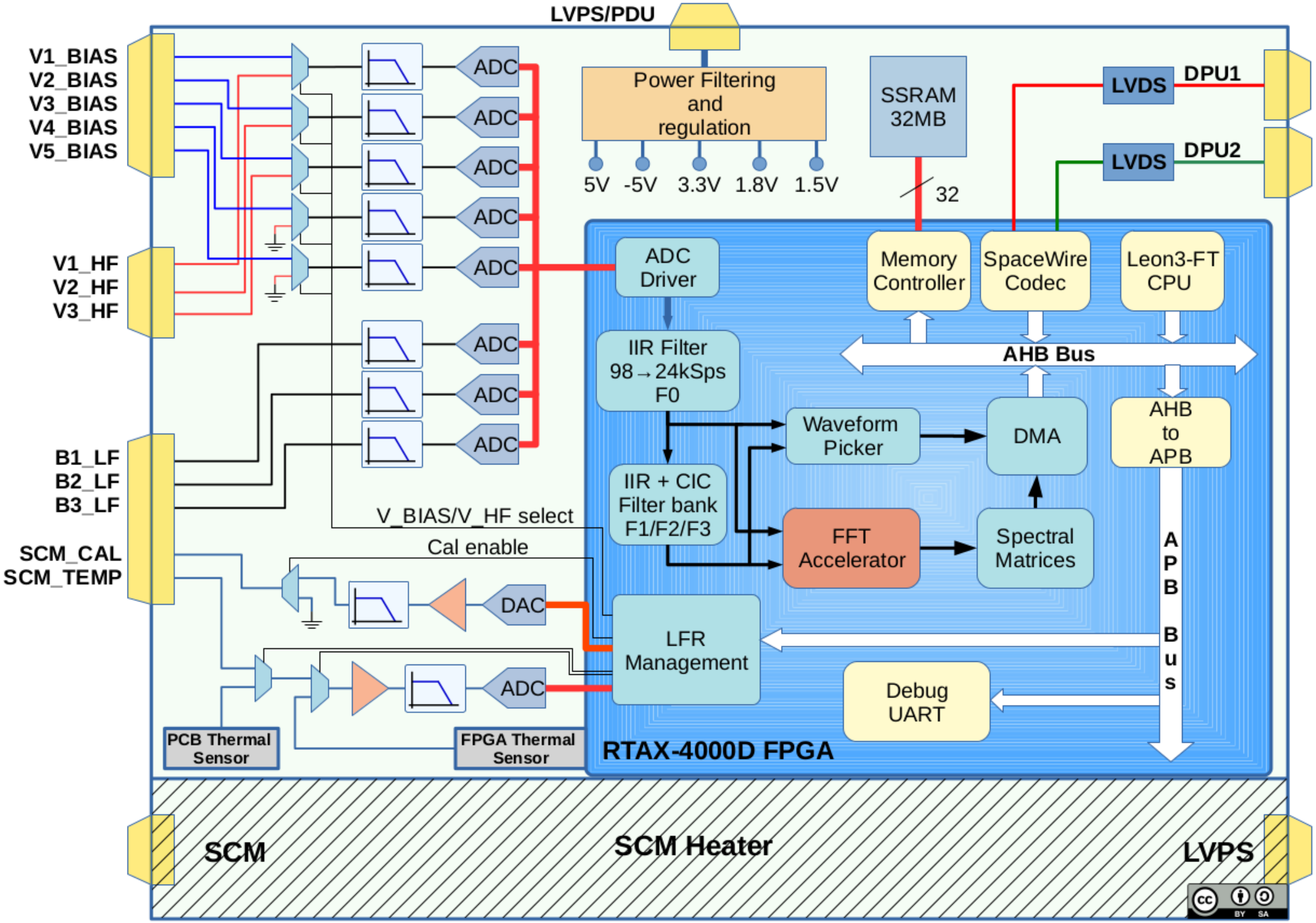

LFR Decimation and Processing Strategy

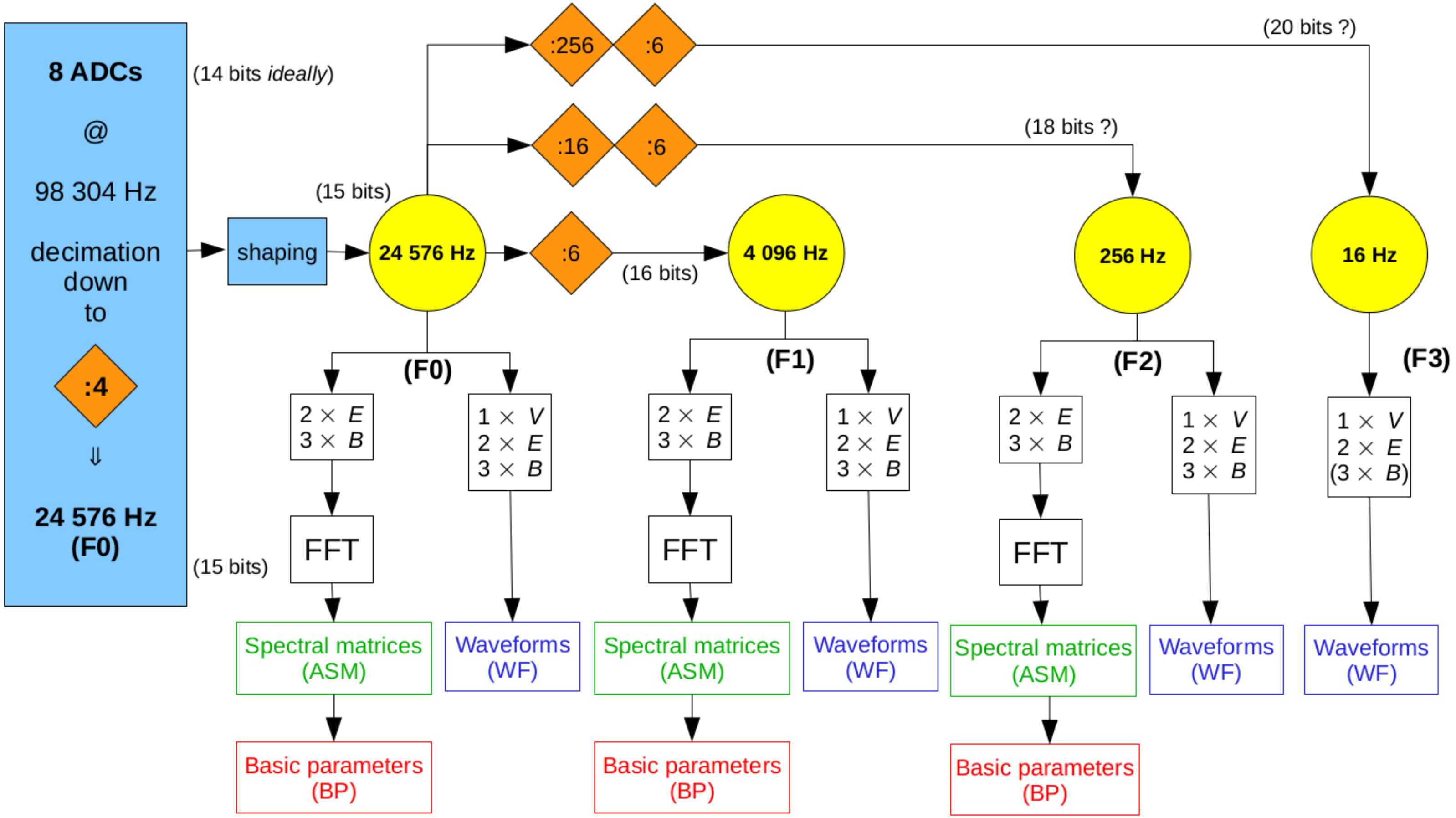

BIAS 5 outputs and the LFR R-parameters

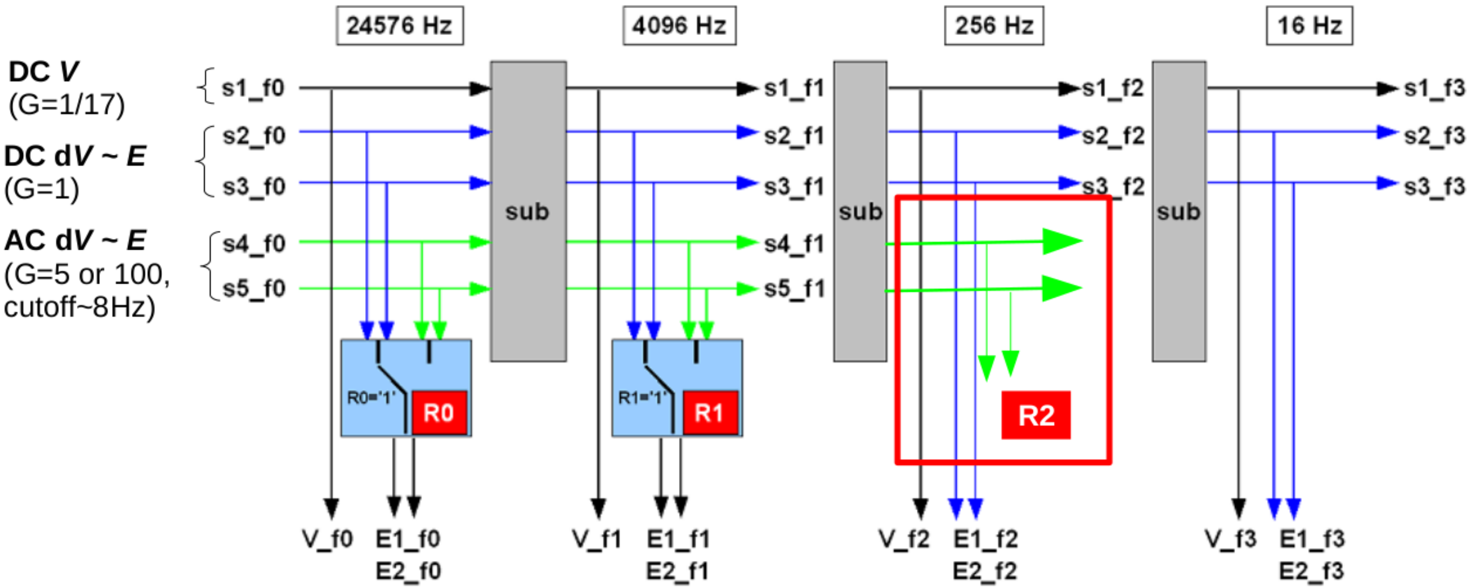

LFR current set of Basic Parameters

"Instantaneous" 5 x 5 spectral matrix
(256-point FFT)

$$\mathbf{SM}\left(\omega_j^{(m)}\right) = \begin{bmatrix} B_1B_1^* & B_1B_2^* & B_1B_3^* & B_1E_1^* & B_1E_2^* \\ cc & B_2B_2^* & B_2B_3^* & B_2E_1^* & B_2E_2^* \\ cc & cc & B_3B_3^* & B_3E_1^* & B_3E_2^* \\ cc & cc & cc & E_1E_1^* & E_1E_2^* \\ cc & cc & cc & cc & E_2E_2^* \end{bmatrix}$$

m = 0, 1, 2
for F0, F1, F2

Time Averaged Spectral Matrix (ASM)

$$\mathbf{ASM}\left(\omega_j^{(m)}\right) = \frac{1}{N_{SM}^{(m)}} \sum_{k=1}^{N_{SM}^{(m)}} \mathbf{SM}_k\left(\omega_j^{(m)}\right) = \langle \mathbf{SM} \rangle_{time}$$

***Frequency* average ...**

$$\mathbf{S}\left(\omega_j^{(m)}\right) = \langle \mathbf{ASM} \rangle_{frequency}$$

... before computations of the BPs
(i.e. wave parameters)

BP1 PB: Power spectrum of the magnetic field (***B***)

BP1 PE: Power spectrum of the electric field (***E***) **=> kcoef**

Mono-**k** assumption: (Means, JGR, 1972) {
BP1 NVEC: Wave normal vector (from ***B***)
BP1 ELLIP: Wave ellipticity estimator (from ***B***)

(Samson & Olson, GJRA, 1980) { BP1 DOP: Wave planarity estimator (from ***B***)

BP1 SX: X_{SRF}(radial)-component of the Poynting vector **=> kcoef**

$\mathbf{n} \times \mathbf{E} = \frac{\omega}{k}\mathbf{B}$ → BP1 VPHI: Phase velocity estimator **=> kcoef (patch needed)**

$\frac{S_{ij}}{\sqrt{S_{ii} S_{jj}}}$ →
BP2 AUTO: Autocorrelations
BP2 CROSS: Normalized cross correlations

LFR spectral frequencies

(1) Depending on the frequency channel, **selection** of 96, 104 or 88 consecutive **frequency bins** among 128 (N_{FFT} = 256) of the *time* averaged spectral matrices.

(2) Then, the ASMs are averaged over packets of N_{freq} (8 or 4) consecutive bins :

$$\Delta f^{(m)} = \frac{f_m}{N_{FFT}} \times N_{freq}$$

$$N_{freq} = 8$$

f_3 = 16 Hz	=>	waveform	[DC, 8Hz]		f_3 / 2.5 = 6.4 Hz
f_2 = 256 Hz	=>	12 frequencies	[6.5Hz, 102.5Hz]	$\Delta f^{(2)}$ = 8 Hz	f_2 / 2.5 = 102.4 Hz
f_1 = 4096 Hz	=>	13 frequencies	[88Hz, 1752Hz]	$\Delta f^{(1)}$ = 128 Hz	f_1 / 2.5 = 1638.4 Hz
f_0 = 24576 Hz	=>	11 frequencies	[1584Hz, 10032Hz]	$\Delta f^{(0)}$ = 768 Hz	f_0 / 2.5 = 9830.4 Hz

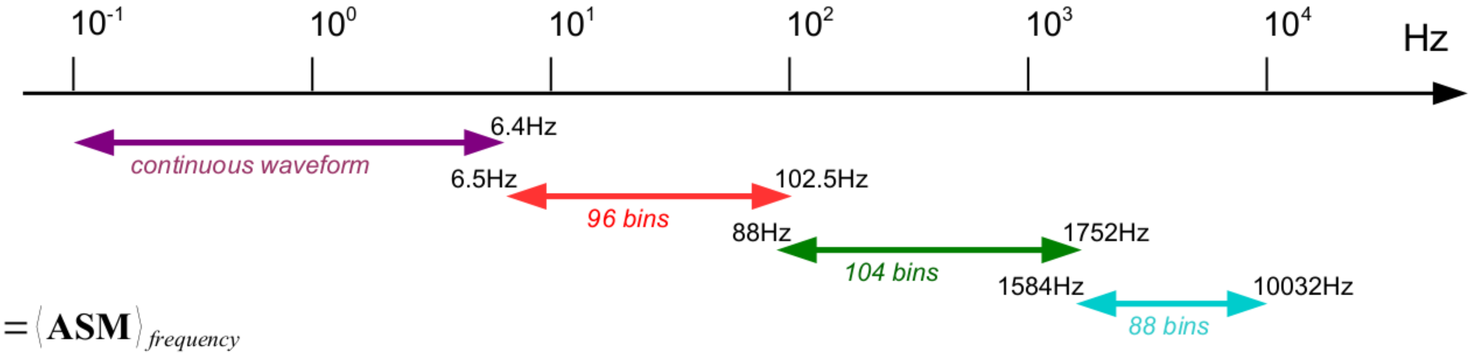

$$S = \langle ASM \rangle_{frequency}$$

Update of the LFR onboard k-coefficients (16 first / 32)

Has been done at the beginning of STP103 (06/07-12/07)

```
:      SOLO_CAL_RPW_BIAS_V202003101607.cdf
       SOLO_CAL_RPW-SCM_SCM-FS-MEB-PFM_V20200428000000.cdf
used:  SOLO_CAL_RCT-LFR-BIAS_V20190123171020.cdf
sed:   SOLO_CAL_RCT-LFR-SCM_V20190123171020.cdf
:      AC_DIFF_G5
       R = 0
       2020-06-18
```

PE : transformation into SRF (2 ortho comp.)
SX : same for B + E-B relative calibration

requency (Hz)	kcoeff_1 (float)	kcoeff_2 (float)	kcoeff_3 (float)	kcoeff_4 (float)	kcoeff_5 (float)	kcoeff_6 (float)	kcoeff_7 (float)	kcoeff_8 (float)	kcoeff_9 (float)	kcoeff_10 (float)	kcoeff_11 (float)	kcoeff_12 (float)	kcoeff_13 (float)	kcoeff_14 (float)	kcoeff_15 (float)	kcoeff_16 (float)
1968.00	1.000000	1.250000	1.000000	-0.000000	0.680709	0.084467	-0.075378	0.002689	-0.006633	-0.004708	-0.828601	-0.100358	-0.615400	-0.121279	-0.684965	-0.072993
2736.00	1.000000	1.250000	1.000000	-0.000000	0.683845	0.046790	-0.077284	0.006480	-0.005590	-0.004755	-0.831959	-0.057230	-0.610072	-0.080905	-0.688697	-0.009801
3504.00	1.000000	1.250000	1.000000	-0.000000	0.684479	0.023171	-0.079053	0.009339	-0.004768	-0.004780	-0.831838	-0.030256	-0.601822	-0.055823	-0.691407	0.035243
4272.00	1.000000	1.250000	1.000000	-0.000000	0.684285	-0.000440	-0.080385	0.012018	-0.003927	-0.004456	-0.830962	-0.002683	-0.592844	-0.031602	-0.694529	0.078141
5040.00	1.000000	1.250000	1.000000	-0.000000	0.683102	-0.032862	-0.080902	0.015643	-0.003207	-0.004357	-0.828408	0.035232	-0.582548	0.000017	-0.694929	0.128425
5808.00	1.000000	1.250000	1.000000	-0.000000	0.679045	-0.077452	-0.080685	0.020638	-0.002670	-0.004105	-0.823017	0.088014	-0.569249	0.042608	-0.689826	0.190891
6576.00	1.000000	1.250000	1.000000	-0.000000	0.670473	-0.129371	-0.079861	0.026565	-0.002390	-0.003748	-0.812267	0.150402	-0.551233	0.090651	-0.677161	0.259483
7344.00	1.000000	1.250000	1.000000	-0.000000	0.660435	-0.171886	-0.078807	0.031303	-0.002101	-0.003724	-0.799841	0.200498	-0.530949	0.130834	-0.663375	0.317959
8112.00	1.000000	1.250000	1.000000	-0.000000	0.660779	-0.168973	-0.079255	0.030848	-0.001279	-0.003575	-0.798949	0.196290	-0.517772	0.135450	-0.669077	0.330162
8880.00	1.000000	1.250000	1.000000	-0.000000	0.677499	-0.077787	-0.082895	0.018871	-0.000068	-0.003632	-0.816823	0.084936	-0.519847	0.073541	-0.715673	0.249207
9648.00	1.000000	1.250000	1.000000	-0.000000	0.681470	0.022690	-0.084661	0.006578	0.000491	-0.003514	-0.819349	-0.036598	-0.515658	0.008594	-0.754707	0.152344
152.00	1.000000	1.250000	1.000000	-0.000000	0.250260	0.644123	-0.026544	-0.050484	-0.003991	-0.011837	-0.308949	-0.769155	-0.238878	-0.832557	-0.266696	-0.894962
280.00	1.000000	1.250000	1.000000	-0.000000	0.435058	0.536410	-0.045370	-0.038012	-0.004918	-0.008762	-0.530177	-0.636836	-0.422869	-0.688790	-0.463289	-0.733262
408.00	1.000000	1.250000	1.000000	-0.000000	0.533893	0.436249	-0.055709	-0.029291	-0.005497	-0.007015	-0.648099	-0.517161	-0.513439	-0.555338	-0.562708	-0.585619
536.00	1.000000	1.250000	1.000000	-0.000000	0.587681	0.359136	-0.061837	-0.022570	-0.006285	-0.006126	-0.713384	-0.424653	-0.558237	-0.453699	-0.611799	-0.472014
664.00	1.000000	1.250000	1.000000	-0.000000	0.618808	0.300719	-0.065342	-0.017659	-0.007364	-0.006185	-0.751394	-0.355742	-0.581250	-0.378724	-0.638215	-0.387033
792.00	1.000000	1.250000	1.000000	-0.000000	0.638057	0.256898	-0.067508	-0.013749	-0.007346	-0.005052	-0.774980	-0.303034	-0.594074	-0.323367	-0.652844	-0.323797
920.00	1.000000	1.250000	1.000000	-0.000000	0.650217	0.222509	-0.069381	-0.010659	-0.007270	-0.004845	-0.790133	-0.262800	-0.601775	-0.280832	-0.661824	-0.274364
1048.00	1.000000	1.250000	1.000000	-0.000000	0.659008	0.194906	-0.070656	-0.007736	-0.007396	-0.004562	-0.800838	-0.229373	-0.606966	-0.246803	-0.668286	-0.234006
1176.00	1.000000	1.250000	1.000000	-0.000000	0.665408	0.169230	-0.071854	-0.006071	-0.007568	-0.004507	-0.809481	-0.199492	-0.610956	-0.217468	-0.673320	-0.198444
1304.00	1.000000	1.250000	1.000000	-0.000000	0.670761	0.146243	-0.072662	-0.003866	-0.007289	-0.004516	-0.815947	-0.172497	-0.614190	-0.191600	-0.677752	-0.167006
1432.00	1.000000	1.250000	1.000000	-0.000000	0.674564	0.125896	-0.073488	-0.001698	-0.007126	-0.004639	-0.820815	-0.148492	-0.616342	-0.169058	-0.680765	-0.139056
1560.00	1.000000	1.250000	1.000000	-0.000000	0.677124	0.111511	-0.073890	-0.000368	-0.007175	-0.004652	-0.823828	-0.131910	-0.616715	-0.152930	-0.682387	-0.117971
1688.00	1.000000	1.250000	1.000000	-0.000000	0.677909	0.106444	-0.074376	0.000250	-0.006978	-0.004553	-0.824805	-0.125884	-0.615684	-0.145642	-0.682700	-0.106756
10.50	1.000000	1.250000	1.000000	-0.000000	-0.064163	0.691371	0.005238	-0.049219	0.001012	-0.010796	0.052509	-0.788477	0.071794	-0.856683	0.075569	-0.916724
18.50	1.000000	1.250000	1.000000	-0.000000	-0.138377	0.678801	0.008808	-0.050425	0.004210	-0.011572	0.136663	-0.788797	0.162978	-0.855399	0.174421	-0.916848
26.50	1.000000	1.250000	1.000000	-0.000000	-0.118979	0.682794	0.007025	-0.049553	0.001158	-0.010515	0.115928	-0.798322	0.146259	-0.866676	0.156269	-0.931405
34.50	1.000000	1.250000	1.000000	-0.000000	-0.086301	0.687445	0.004599	-0.050711	0.001742	-0.010776	0.079182	-0.809000	0.110229	-0.880463	0.116501	-0.944506
42.50	1.000000	1.250000	1.000000	-0.000000	-0.051160	0.691451	0.002795	-0.050467	0.002297	-0.008438	0.042965	-0.813893	0.074655	-0.888435	0.078498	-0.951999
50.50	1.000000	1.250000	1.000000	-0.000000	-0.017434	0.690637	-0.003165	-0.057706	0.007160	-0.013982	0.009704	-0.816750	0.037321	-0.898358	0.038160	-0.959488
58.50	1.000000	1.250000	1.000000	-0.000000	0.008883	0.692317	-0.001998	-0.051320	0.002576	-0.010018	-0.026732	-0.817230	0.010392	-0.894188	0.008285	-0.959643
66.50	1.000000	1.250000	1.000000	-0.000000	0.033912	0.691814	-0.006235	-0.051648	0.000089	-0.011058	-0.056269	-0.820826	-0.015915	-0.893520	-0.019992	-0.958181
74.50	1.000000	1.250000	1.000000	-0.000000	0.058759	0.689708	-0.008406	-0.051508	-0.000637	-0.010220	-0.085366	-0.818306	-0.041164	-0.890868	-0.047973	-0.954232
82.50	1.000000	1.250000	1.000000	-0.000000	0.081055	0.688097	-0.011295	-0.049474	-0.000468	-0.010783	-0.111820	-0.815674	-0.063871	-0.888986	-0.072991	-0.953335
90.50	1.000000	1.250000	1.000000	-0.000000	0.103966	0.685133	-0.012776	-0.050548	-0.001181	-0.011071	-0.137918	-0.812970	-0.087822	-0.884208	-0.099221	-0.947926
98.50	1.000000	1.250000	1.000000	-0.000000	0.122452	0.682203	-0.015249	-0.049152	-0.001474	-0.010516	-0.159991	-0.808639	-0.107694	-0.880608	-0.120736	-0.945213

11 F0 + 13 F1 + 12 F2 = 36 frequency bins

Computation of the k-coefficients for PE

Power spectrum of the electric field

$$\langle E_{Y'} E^*_{Y'} + E_{Z'} E^*_{Z'} \rangle = \left\langle {}^{\mathrm{T}}\mathbf{E}_{ANT} \cdot \frac{1}{|A_{1Y'} A_{2Z'} - A_{1Z'} A_{2Y'}|^2} \begin{bmatrix} |A_{2Y'}|^2 + |A_{2Z'}|^2 & -A^*_{1Y'} A_{2Y'} - A^*_{1Z'} A_{2Z'} \\ -A_{1Y'} A^*_{2Y'} - A_{1Z'} A^*_{2Z'} & |A_{1Y'}|^2 + |A_{1Z'}|^2 \end{bmatrix} \cdot \mathbf{E}^*_{ANT} \right\rangle$$

$$= \frac{|A_{2Y'}|^2 + |A_{2Z'}|^2}{|A_{1Y'} A_{2Z'} - A_{1Z'} A_{2Y'}|^2} \left(S_{44} + \frac{|A_{1Y'}|^2 + |A_{1Z'}|^2}{|A_{2Y'}|^2 + |A_{2Z'}|^2} S_{55} - 2\,\Re\left[\frac{A^*_{1Y'} A_{2Y'} + A^*_{1Z'} A_{2Z'}}{|A_{2Y'}|^2 + |A_{2Z'}|^2} S_{45} \right] \right)$$

Calibration factor

$$\Rightarrow \quad \mathrm{PE} = S_{44}\, k^{pe}_{44} + S_{55}\, k^{pe}_{55} + \Re\left[S_{45}\, k^{pe}_{45} \right]$$

with

$$\begin{cases} k^{pe}_{44} = 1 \\ k^{pe}_{55} = \dfrac{|A_{1Y'}|^2 + |A_{1Z'}|^2}{|A_{2Y'}|^2 + |A_{2Z'}|^2} \\ k^{pe}_{45} = -2\, \dfrac{A^*_{1Y'} A_{2Y'} + A^*_{1Z'} A_{2Z'}}{|A_{2Y'}|^2 + |A_{2Z'}|^2} \end{cases}$$

WARNING: The TF of BIAS and LFR are implicitly embodied in the TF matrix of ANT (just a common calibration factor)

Computation of the k-coefficients for SX

X_{SRF}-component of the Poynting vector

$$\langle S_{X'} \rangle = \langle (\mathbf{E} \times \mathbf{B^*})_{X'} \rangle = \langle E_{Y'} B^*_{Z'} \rangle - \langle E_{Z'} B^*_{Y'} \rangle$$

$$= \left\langle \frac{A_{2Z'} E_1 - A_{1Z'} E_2}{A_{1Y'} A_{2Z'} - A_{1Z'} A_{2Y'}} \frac{1}{C^*_{1Y}} \tilde{m}^*_{Z'j} B^*_j \right\rangle - \left\langle \frac{-A_{2Y'} E_1 + A_{1Y'} E_2}{A_{1Y'} A_{2Z'} - A_{1Z'} A_{2Y'}} \frac{1}{C^*_{1Y}} \tilde{m}^*_{Y'j} B^*_j \right\rangle$$

$$= \frac{\left(A_{2Y'} \tilde{m}^*_{Y'j} + A_{2Z'} \tilde{m}^*_{Z'j}\right) \langle E_1 B^*_j \rangle - \left(A_{1Y'} \tilde{m}^*_{Y'j} + A_{1Z'} \tilde{m}^*_{Z'j}\right) \langle E_2 B^*_j \rangle}{\left(A_{1Y'} A_{2Z'} - A_{1Z'} A_{2Y'}\right) C^*_{1Y}}$$

Calibration factor

$$= \frac{\sqrt{|A_{2Y'}|^2 + |A_{2Z'}|^2}}{\left(A_{1Y'} A_{2Z'} - A_{1Z'} A_{2Y'}\right) C^*_{1Y}} \left[\frac{A_{2Y'} \tilde{m}^*_{Y'j} + A_{2Z'} \tilde{m}^*_{Z'j}}{\sqrt{|A_{2Y'}|^2 + |A_{2Z'}|^2}} S_{4j} - \frac{A_{1Y'} \tilde{m}^*_{Y'j} + A_{1Z'} \tilde{m}^*_{Z'j}}{\sqrt{|A_{2Y'}|^2 + |A_{2Z'}|^2}} S_{5j} \right]$$

$$\Rightarrow \quad \mathrm{SX'} = S_{41} k^{sx'}_{41} + S_{42} k^{sx'}_{42} + S_{43} k^{sx'}_{43} + S_{51} k^{sx'}_{51} + S_{52} k^{sx'}_{52} + S_{53} k^{sx'}_{53}$$

with

$$\begin{cases} k^{sx'}_{4j} = + \dfrac{A_{2Y'} \tilde{m}^*_{Y'j} + A_{2Z'} \tilde{m}^*_{Z'j}}{\sqrt{|A_{2Y'}|^2 + |A_{2Z'}|^2}} \times \exp\left[i \left(\varphi_{C_{1Y}} - \varphi_{A_{1Y'} A_{2Z'} - A_{1Z'} A_{2Y'}} \right) \right] & j = 1, 2, 3 \\ k^{sx'}_{5j} = - \dfrac{A_{1Y'} \tilde{m}^*_{Y'j} + A_{1Z'} \tilde{m}^*_{Z'j}}{\sqrt{|A_{2Y'}|^2 + |A_{2Z'}|^2}} \times \exp\left[i \left(\varphi_{C_{1Y}} - \varphi_{A_{1Y'} A_{2Z'} - A_{1Z'} A_{2Y'}} \right) \right] \end{cases}$$

WARNING: As for ANT, the TF of LFR is implicitly embodied in the TF matrix of SCM (just a common calibration factor)

LFR Selected Burst Mode 2 & BURST mode

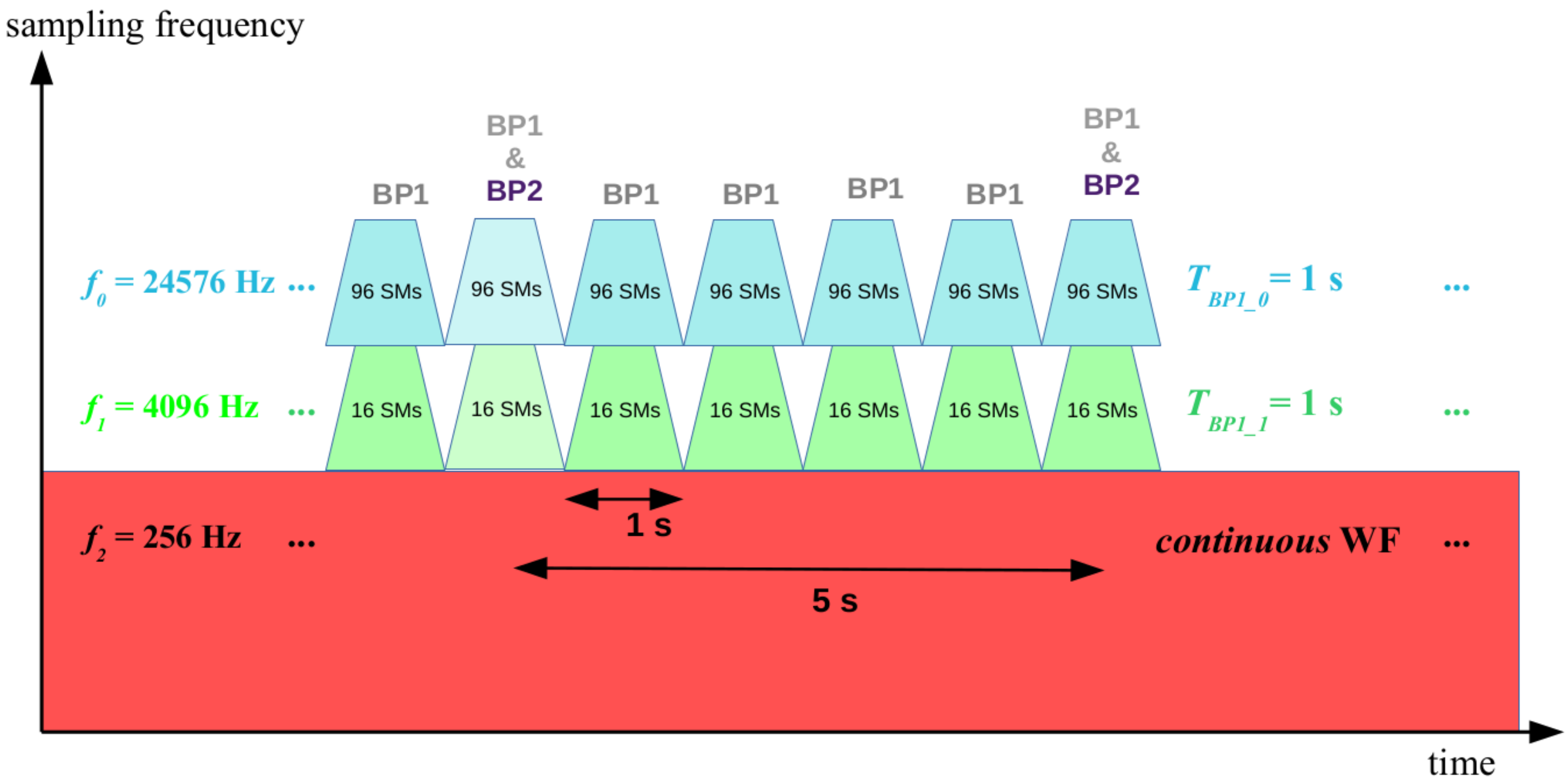

LFR Selected Burst Mode 1

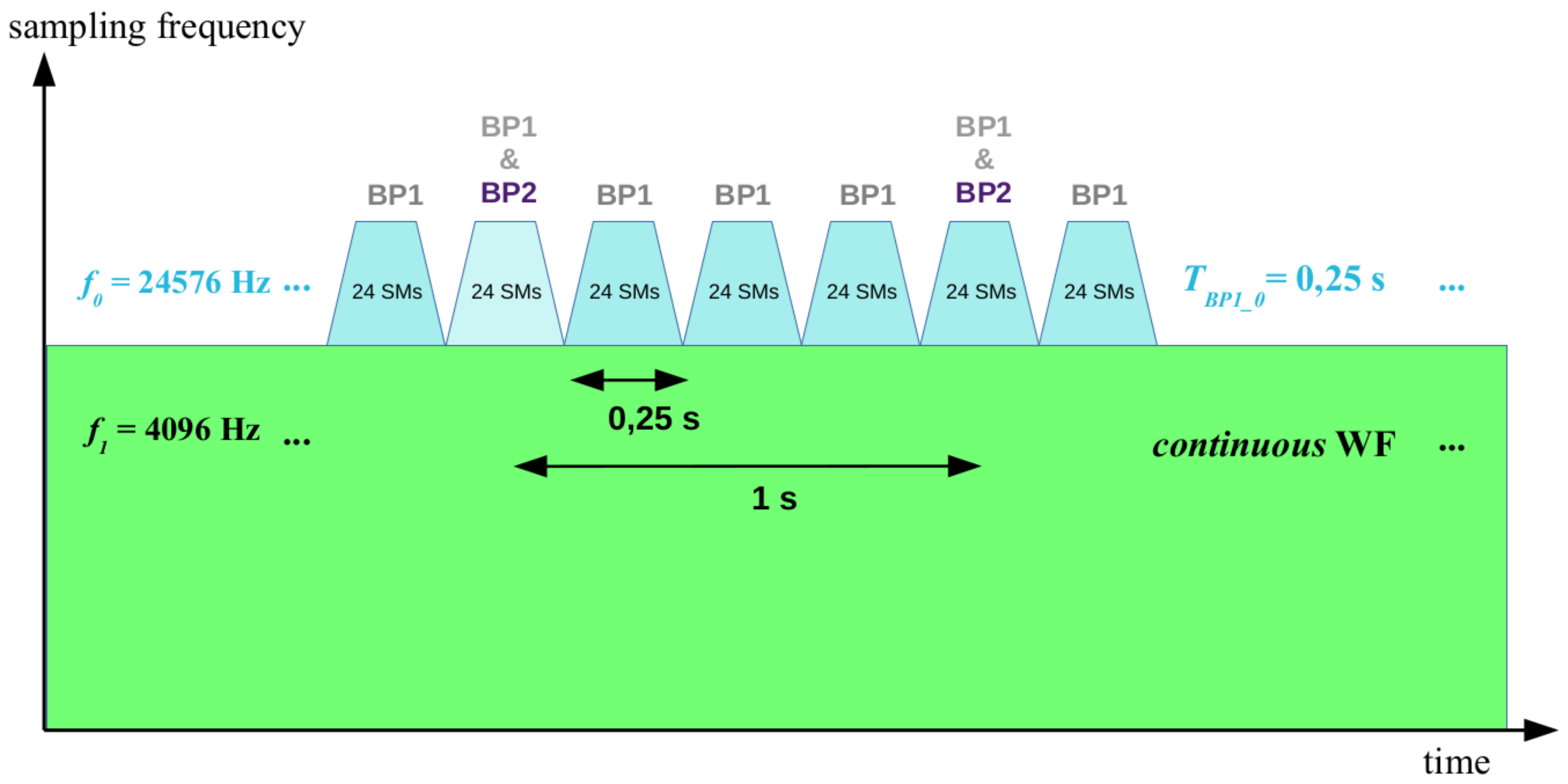

Overview of the A&A special issue papers (1)

- **Whistler waves**

Observations of whistler mode waves by the Solar Orbiter RPW Low Frequency Receiver (LFR): in-flight performance and first results, Chust, T., M. Kretzschmar, D. B. Graham et al., A & A, 2021.

Whistler waves observed by Solar Orbiter / RPW between 0.5 AU and 1 AU, Kretzschmar, M., T. Chust, V. Krasnoselskikh et al., A & A, 2021.

Whistler instability driven by the suprathemal electron deficit in the solar wind, High-cadence Solar Orbiter observations, Berčič, L., D. Verscharen, C. J. Owen, , A & A, 2021.

- **DC electric field and S/C potential measurements**

Solar wind current sheets and deHoffmann-Teller analysis: First results of DC electric field measurements by Solar Orbiter, Steinvall, K., Yu. V. Khotyaintsev, G. Cozzani et al, A & A, 2021.

Density Fluctuations Associated with Turbulence and Waves, First Observations by Solar Orbiter, Khotyaintsev , Yu. V., D. B. Graham, A. Vaivads, et al, A & A, 2021.

Statistical study of electron density turbulence and ion-cyclotron waves in the inner heliosphere: Solar Orbiter observations, Carbone, F., L. Sorriso-Valvo, Yu. V. Khotyaintsev et al, A & A, 2021.

Study of two interacting Interplanetary Coronal Mass Ejections encountered by Solar Orbiter during its first perihelion passage, Observations and modeling, Telloni D., C. Scolini, C. Möstl et al, A & A, 2021.

Overview of the A&A special issue papers (2)

- **Venus flyby**

Solar Orbiter's first Venus flyby: observations from the Radio and Plasma Wave instrument, Hadid, L. Z., N. J. T. Edberg, T. Chust et al., A & A, 2021.

Analysis of multi-scale structures at the quasi-perpendicular Venus bow shock, Results from Solar Orbiter's first Venus flyby, Dimmock, A. P., Yu. V. Khotyaintsev, A. Lalti et al., A & A, 2021.

Energetic Ions in the Venusian System: Insights from the First Solar Orbiter Flyby, Allen R. C., I. Cernuda, D. Pacheco, et al, A & A, 2021.

- **Ion acoustic waves**

Kinetic Electrostatic Waves and their Association with Current Structures in the Solar Wind, Graham, D. B., Yu. V. Khotyaintsev, A. Vaivads et al, A & A, 2021.

- **Cometary observations**

Waves and structures from Solar Orbiter's encounter with the tail of comet C/2019 Y4 (ATLAS); signatures from magnetic field draping and cometary pick-up ion instabilities, L. Matteini, R. Laker, T. Horbury et al, A & A, 2021.

- **Overview of the RPW instrument suite**

First observations and performance of the RPW instrument onboard the Solar Orbiter mission, Maksimovic , M., J. Souček, T. Chust, et al, A & A, 2021.